Cell Genomics

Article

Sequential activation of transcription factors promotes liver regeneration through specific and developmental enhancers

Graphical abstract

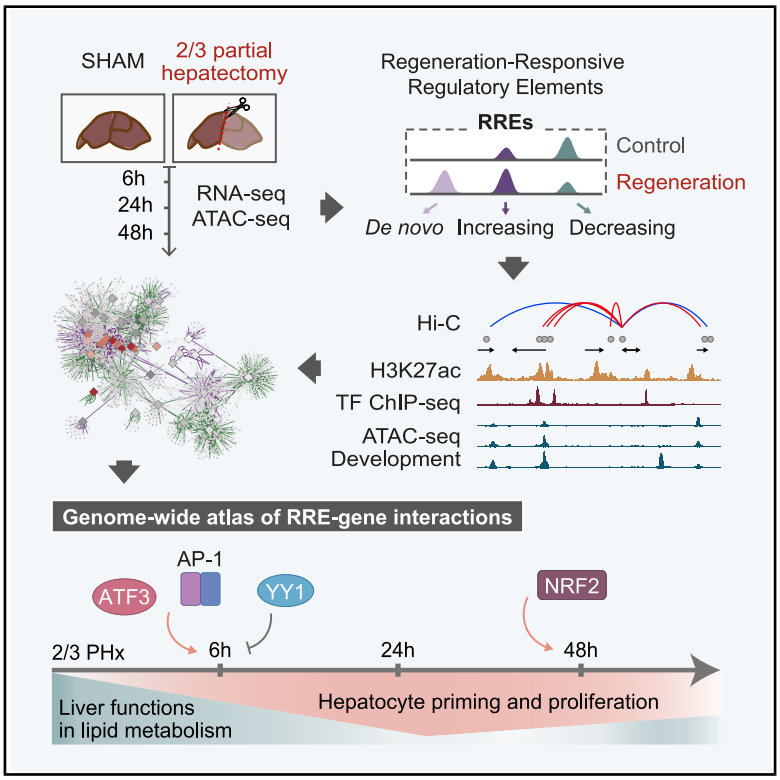

Highlights

- Regeneration-responsive regulatory elements (RREs) were identified in early liver regeneration
- RRE-gene interaction atlas reveals shift from lipid metabolism to proliferative programs
- RREs comprise both regeneration-specific and reactivated developmental enhancers
- Integrative genomic analysis generates GRN with a transcription-factor-activation cascade

Authors

Palmira Llorens-Giralt, Marina Ruiz-Romero, Ramil Nurtdinov, ..., Florenci Serras, Isabel Fabregat, Montserrat Corominas

Correspondence

mcorominas@ub.edu

In brief

Llorens-Giralt et al. study how liver cells respond to partial hepatectomy by examining changes in gene activity and chromatin accessibility. They create a functional regulatory map of early liver regeneration and identify key elements controlling specific gene programs essential for liver repair and growth.

Llorens-Giralt et al., 2025, Cell Genomics *5*, 100887
July 9, 2025
https://doi.org/10.1016/j.xgen.2025.100887

CellPress

Cell Genomics

CellPress
OPEN ACCESS

Article

Sequential activation of transcription factors promotes liver regeneration through specific and developmental enhancers

Palmira Llorens-Giralt,[1,6] Marina Ruiz-Romero,[2,6] Ramil Nurtdinov,[2] Macarena Herranz-Itúrbide,[3,4] Guillermo P. Vicent,[5] Florenci Serras,[1] Isabel Fabregat,[3,4] and Montserrat Corominas[1,7,*]

[1]Department of Genetics, Microbiology and Statistics, Faculty of Biology and Institute of Biomedicine (IBUB), University of Barcelona, Diagonal 643, 08028 Barcelona, Catalonia, Spain

[2]Centre for Genomic Regulation (CRG), The Barcelona Institute for Science and Technology (BIST), Dr. Aiguader 88, Barcelona 08003, Spain

[3]TGF-beta and Cancer Group, Oncobell Program, Bellvitge Biomedical Research Institute (IDIBELL), Av. Granvia de l'Hospitalet 199, 08908 L'Hospitalet de Llobregat, Barcelona, Spain

[4]Oncology Program, National Biomedical Research Institute on Liver and Gastrointestinal Diseases (CIBEREHD), Instituto de Salud Carlos III, Madrid, Spain

[5]Molecular Biology Institute of Barcelona, Consejo Superior de Investigaciones Científicas (IBMB-CSIC), Baldiri Reixac 4-8, 08028 Barcelona, Spain

[6]These authors contributed equally

[7]Lead contact

*Correspondence: mcorominas@ub.edu

https://doi.org/10.1016/j.xgen.2025.100887

SUMMARY

The mammalian liver exhibits remarkable regenerative capabilities after injury or resection. Central to this process is the precise modulation of gene expression, driven by changes in chromatin structure and the temporal activation of distal regulatory elements. In this study, we integrated chromatin accessibility and transcriptomic data after partial hepatectomy in mice. We show that the expression of crucial regeneration genes is orchestrated by a diverse array of *cis*-regulatory elements, including regeneration-specific enhancers and enhancers repurposed from various developmental stages. These enhancers collaborate to activate the transcriptional programs required for hepatocyte priming and proliferation, with their activity initially regulated by the activator protein-1 (AP-1) complex and ATF3, and subsequently by nuclear factor erythroid 2 (NFE2)-related factor 2 (NRF2) during proliferation. Our results also indicate that hepatic regeneration involves the repression of enhancers regulating liver-specific metabolic functions, particularly those involved in lipid metabolism. This study provides a genome-wide atlas of enhancer-gene interactions, offering new insights into the regulatory mechanisms underlying liver regeneration.

INTRODUCTION

Regenerative capacity varies greatly, not only across species but also between tissues, organs, and developmental stages within the same species. The evolutionary conservation of regeneration-associated genes suggests that variations in regenerative ability arise from differences in how these genes are regulated after injury, rather than simply whether they are present.[1,2] Genome-wide chromatin profiling has identified *cis*-regulatory elements activated by injury that orchestrate regenerative transcriptional programs. These regeneration-responsive elements have been characterized in regenerating zebrafish heart,[3,4] fins,[5,6] and spinal cord,[7] as well as *Drosophila* wing imaginal discs.[8,9] In mice, similar enhancer activity has been observed in skeletal muscle,[10] Schwann cells,[11] skin stem cells,[12,13] and heart.[14,15] Recent studies show that regeneration-responsive enhancers can be engineered to drive pro-regenerative gene expression specifically in damaged tissues via transgenic models or viral vectors.[5,16] These elements are transiently activated after injury and deactivate once repair is complete, minimizing potential tumorigenic risk.

In vertebrates, the liver has remarkable regenerative capacity, fully restoring mass and function after injury or partial hepatectomy (PHx).[17,18] Under normal conditions, hepatocytes are quiescent, but within 4 h after PHx, approximately 95% re-enter the cell cycle.[19,20] This is triggered by a cytokine-driven priming phase, which induces proliferation genes and represses liver-specific differentiation genes.[21] Growth factors then promote cell-cycle progression, leading to mitosis by 48 h.[18] Proliferation is later arrested by transforming growth factor (TGF)-β and activins via tumor-suppressor gene activation, thus preserving liver size and homeostasis.[19,22]

Understanding the regulatory mechanisms of liver regeneration could have profound implications for regenerative medicine.

Although genetic and epigenetic drivers have been described,[23,24] the role of specialized enhancers in controlling pro-regenerative genes remains unclear. Recent studies have explored histone modifications and DNA methylation after PHx,[21,25–27] chromatin accessibility dynamics after toxicity in a model of hereditary tyrosinemia,[28] and epigenetic changes during biliary reprogramming.[29] Single-cell approaches have further revealed the gene regulatory networks (GRNs) of hepatic cells during the later stages of liver regeneration after PHx.[30–32]

However, our understanding of how early signals reshape gene expression and chromatin architecture during liver regeneration remains incomplete. Although recent evidence suggests that hepatocytes adopt a fetal-like chromatin and transcriptional state,[30,31] it remains unclear whether regeneration relies solely on reactivating developmental networks or involves a distinct regeneration-specific program.

Here, we profiled gene expression and chromatin accessibility during the early stages of liver regeneration in mice. Using an integrative algorithm that combines chromatin state and 3D conformation data, we identified regulatory elements specifically activated after PHx and predicted their target genes. This analysis revealed reduced accessibility at regions associated with liver-specific metabolic genes, alongside increased accessibility at regulatory elements linked to pro-proliferative genes. Additionally, we constructed a GRN that uncovered a cascade of transcription factor (TF) activation, highlighting key TFs that are upregulated and/or essential for regeneration. Our findings further suggest that liver regeneration involves both regeneration-specific enhancers and reactivated developmental enhancers, each governed by distinct regulatory mechanisms and associated with different biological functions.

RESULTS

Liver regeneration-responsive regulatory elements

To identify regulatory elements involved in early liver regeneration, we performed genome-wide transcriptomics and chromatin accessibility profiling on mouse livers at 6, 24, and 48 h after sham (control) or two-thirds (2/3) PHx (REG) surgery (Figure 1A), using the same samples for RNA sequencing (RNA-seq)[33] and assay for transposase-accessible chromatin using sequencing (ATAC-seq). The time points selected correspond with critical stages in liver regeneration, marking the end of the priming stage (6 h), the entry of hepatocytes into the S phase of the cell cycle (24 h), and their progression into mitosis (48 h). The latter two fall within the proliferation or progression phase of liver regeneration.[17,18]

First, we used correspondence analysis and association plots[34] to cluster the expressed genes (11,512 genes) (Figures S1A–S1C). This method enabled us to identify the genes that were differentially expressed either in the control livers or at specific time points during regeneration (6, 24, or 48 h post PHx) (Figures 1B and 1C), as well as those that were co-expressed across different regeneration time points (Figures S1D and S1E; Table S1). The cluster corresponding to the initial stage of regeneration (REG 6 h) showed the highest gene count, with 1,375 genes exhibiting significantly higher expression levels at 6 h compared with the other conditions (Figures 1B, 1C, and S1C). As previously reported,[35] we found that the gene expression profile at the initial time point post-PHx resembled that of the corresponding sham-operated control, albeit with a tendency toward increased expression levels in regeneration (Figures S1A and S1B). This similarity is likely due to the disturbance in gene expression caused by surgical stress and anesthesia. The other gene clusters specific to regeneration encompassed approximately 200–400 genes each (Figures 1B, 1C, S1D, and S1E). Notably, the cluster of genes co-expressed across regeneration (REG 6-24-48 h) comprised only 227 genes (Figures S1D and S1E). This suggests a dynamic transcriptomic profile with sequential gene activation and repression.

Gene Ontology (GO) analysis revealed that control livers were enriched for lipid-related pathways, including steroid and bile acid metabolism, as well as lipid catabolism (Figure 1D), consistent with known suppression of bile acid synthesis during liver regeneration to prevent cytotoxicity.[36] In contrast, genes associated with cell signaling, cell response, proliferation, and mitosis were specifically enriched in particular regeneration clusters, indicating a sequential activation during regeneration (Figure 1D). For instance, the REG 6 h cluster showed unique enrichment for hepatocyte growth factor (HGF) response and phospholipid biosynthesis, whereas several terms related to the mitotic cell cycle were significantly enriched among the REG 48 h cluster. HGF is among the earliest mitogens detected after PHx in mice and plays a crucial role in liver regeneration,[37] while the synthesis of phospholipids is essential for generating new cell membranes and, therefore, for hepatocyte proliferation during regeneration.[38] These transcriptomic changes after PHx accurately reflect known physiological events underlying early liver regeneration.[25,35]

Next, we examined the changes in chromatin accessibility that could trigger these transcriptional profiles by mapping open regions by ATAC-seq in livers at 6, 24 and 48 h after sham surgery or 2/3 PHx (Figures S2A and S2B). We performed pairwise comparisons between control and regeneration at each time point ($|FC| > 1.7$) and identified more than 17,000 differentially accessible chromatin regions in at least one time point, compared with 60,000 that were non-differentially accessible (NDA). Differentially accessible regions were classified into *de novo*, increasing or decreasing peaks: *de novo* peaks were open regions detected exclusively during regeneration; increasing peaks were regions already open in the control but displaying higher accessibility during regeneration; and decreasing peaks were regions with lower accessibility during regeneration (Figures 2A and 2B). We observed a similar number of decreasing peaks over time, with nearly 4,000 identified at each time point (Figure 2C). In contrast, the number of increasing peaks slightly increased over time (1,717 peaks at 6 h, 2,935 peaks at 24 h, and 2,886 peaks at 48 h after PHx) and *de novo* peaks were more enriched at 6 h and 48 h compared with 24 h: 427, 449, and 255 peaks, respectively (Figure 2C). Differentially accessible peaks from all classes were mostly time point specific (Figure S2C), indicating that chromatin architecture changes throughout the regenerative process.

We next classified ATAC-seq peaks by distance to the nearest transcription start site as promoter (±500 bp), proximal (<1 kb), or distal (≥1 kb) regions. In comparison with NDA, the *de novo*,

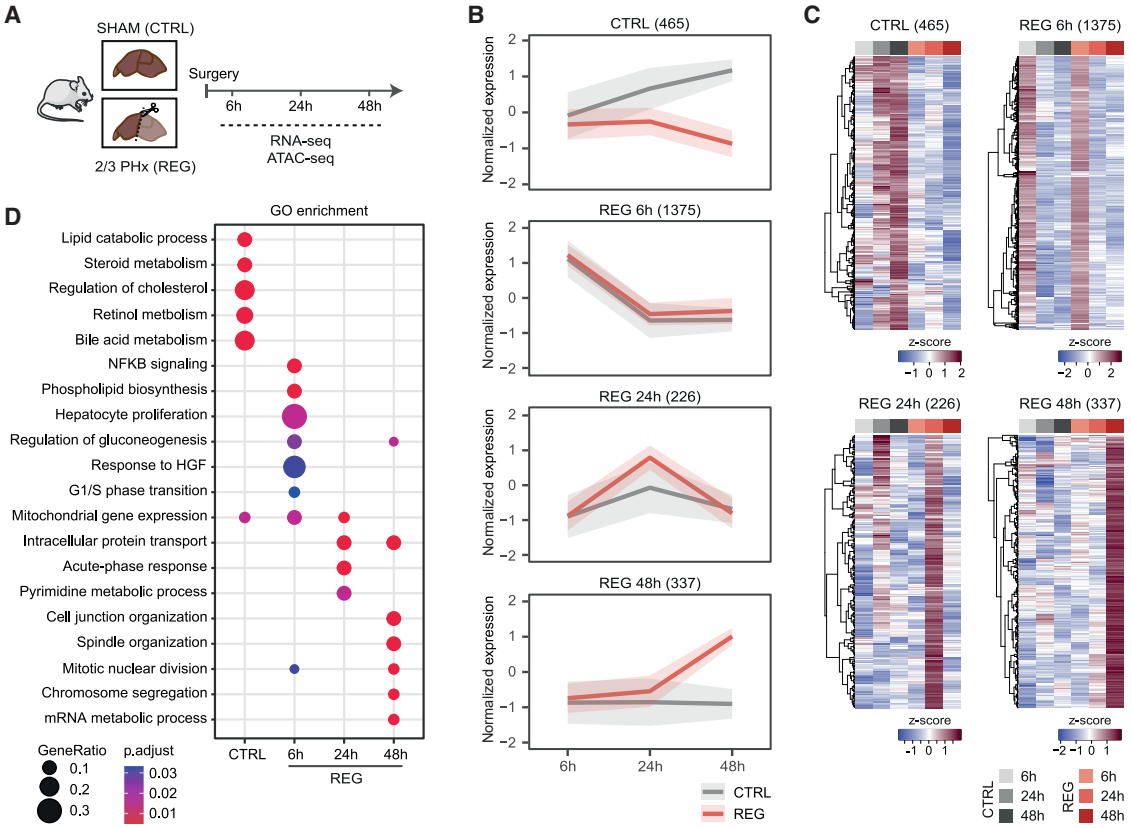

Figure 1. Gene expression profiles of liver regeneration after PHx

(A) Experimental design. Male and female mice aged 8–16 weeks underwent either sham surgery (SHAM/CTRL) or 2/3 PHx/REG. Mice were euthanized at 6, 24, or 48 h post surgery, and liver lobes were snap-frozen. RNA-seq data were obtained from Herranz-Itúrbide et al.[33] and the same biological samples were used for ATAC-seq.

(B) Standardized expression profiles of four gene clusters: control, 6 h, 24 h, and 48 h after PHx. Gene expression values are *Z*- score normalized. Mean expression (line) ± standard deviation (shade) and gene counts are shown per cluster.

(C) Heatmaps of expression for each cluster. Columns represent conditions (averaged across replicates), and gene expression is *Z*- score normalized, gene order was established by hierarchical clustering. Gene counts per cluster are shown above.

(D) GO terms enriched in each gene cluster (one-sided Fisher's exact test $p_{adjusted} < 0.05$). NFKB, nuclear factor κ-light-chain-enhancer of activated B cells. See also Figure S1.

increasing, and decreasing peaks tended to be more prevalent in the distal regions (>90%), primarily within introns and intergenic regions, while less than 7% were in promoters and only 2%–3% within proximal regions (Figures 2D and S2D). Indeed, most promoters remained relatively stable during regeneration, comprising nearly 25% of NDA peaks. Given that distal regions are typically associated with enhancers, these findings suggest that the chromatin response to PHx predominantly involves the modulation of enhancer accessibility.

To further characterize regeneration-responsive regulatory elements (RREs), we integrated ATAC-seq data with H3K27ac profiles from undamaged[39] and regenerating livers,[40] as this histone mark is linked to active enhancers.[41] First, we observed a highly statistically significant overlap (Fisher's exact test, $p = 2.2e^{-16}$) between RREs (extended to 500 bp to incorporate the flanking nucleosomes) and H3K27ac. Approximately 65% of RREs were flanked by H3K27ac enriched regions, further supporting their role as enhancers. We observed that the H3K27ac signature differed for each type of RRE (Figure 2E). Compared with NDA, *de novo* and increasing RREs exhibited a higher proportion of peaks exclusively marked by H3K27ac during regeneration (REG specific). In contrast, decreasing peaks tended to be marked both in control and regeneration or only in the control. While certain *de novo* peaks exhibited regeneration-specific H3K27ac, indicating they can gain acetylation after PHx, most of them were unmarked in all conditions. This suggests that the regulation mediated by these elements may occur independent of this histone tail acetylation. As previously proposed, the active enhancer repertoire cannot be fully characterized by H3K27ac alone.[42]

Switch in chromatin accessibility from RREs linked to homeostatic lipid metabolism to proliferation-associated RREs

To better understand gene regulation during liver regeneration, we mapped genome-wide functional enhancer-gene pairs.

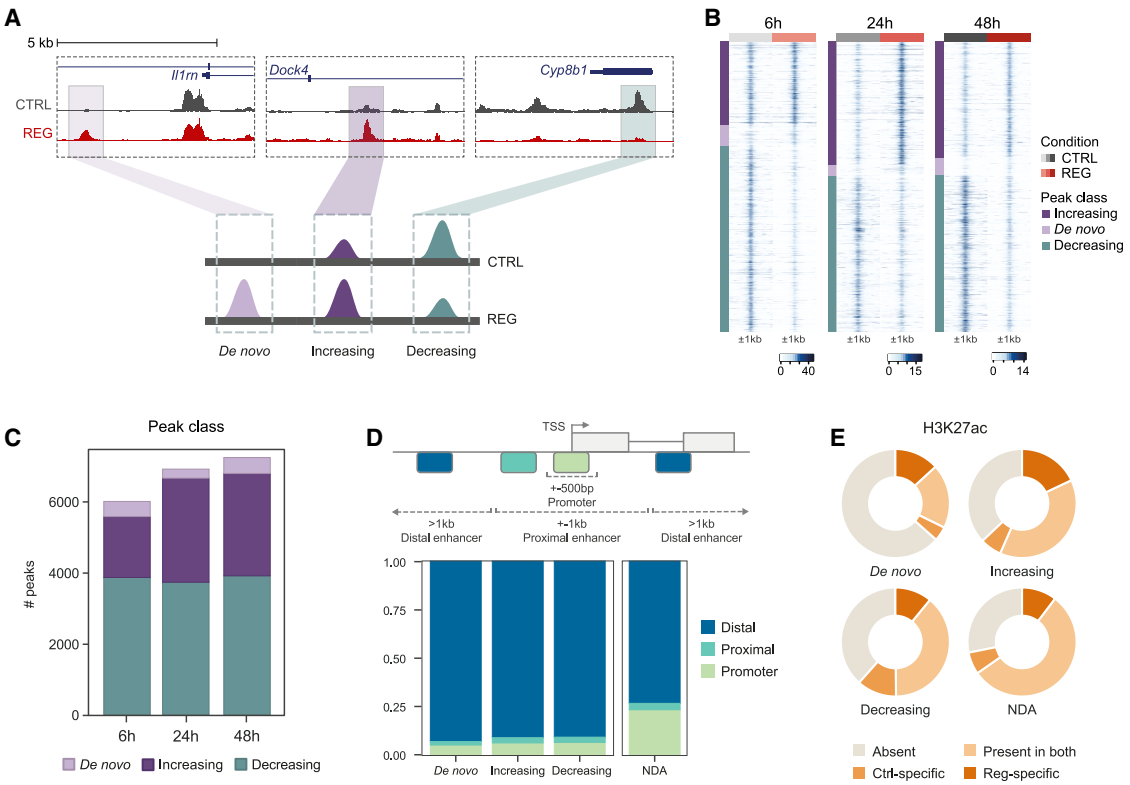

Figure 2. Chromatin accessibility changes during liver regeneration

(A) Genome browser views and schematics of *de novo*, increasing and decreasing peaks.

(B) Quantile normalized ATAC-seq signals ±1 kb from peak summits, grouped by peak class.

(C) Number of differentially accessible peaks per class at each time point.

(D) (Top) Genomic annotation of peaks. (Bottom) Proportion of promoters, proximal, and distal enhancers per class peaks.

(E) H3K27ac presence in control (uninjured) and regeneration (40 h post PHx) livers in NDA peaks and RREs. See also Figure S2.

Proximal enhancers were assigned to the nearest gene, while the target genes of distal enhancers were predicted using the activity-by-contact (ABC) model of enhancer-promoter regulation.[43] Briefly, this model is based on the principle that each enhancer regulates gene expression proportionally to its activity, and the frequency of its interaction with the gene's promoter. The ABC model combines chromatin state data, such as accessibility and histone modifications, to assess enhancer activity, and uses chromosome conformation capture (Hi-C) data to infer contact frequency between enhancers and promoters. This model outperforms simpler alternatives such as distance-based and Hi-C contact-based predictions. For input into the ABC model, we used our ATAC-seq data, publicly available H3K27ac chromatin immunoprecipitation sequencing (ChIP-seq) data from regenerating livers[40] and *in situ* Hi-C and promoter-capture Hi-C data from intact livers.[44]

The ABC algorithm predicted 15,816 distal enhancer-gene pairs, of which 15,499 (97.9%) were associated with expressed genes in at least one condition (Tables S2 and S3). Unlike conventional methods that assign enhancers solely based on the proximity to the nearest gene, the ABC method allowed us to predict the target genes of distal enhancers even when these were located megabases away. For instance, it identified an interaction between two increasing enhancers and a *de novo* enhancer with the promoter of the *Pnpla8* gene, despite being separated by more than 1.2 Mb in the linear genome (Figure 3A). We next assessed the Pearson's correlation coefficient between chromatin accessibility at regeneration-responsive promoters and enhancers and their target gene expression across time points. Promoters showed the highest correlation, followed by proximal and distal enhancers (Figure S3A). Moreover, increasing peaks exhibited significantly stronger correlations than *de novo* or decreasing peaks (Figure S3B). Altogether, these results support the accuracy of ABC-predicted enhancer-gene pairs.

Next, we analyzed the expression of predicted target genes during regeneration and found distinct transcriptional patterns across RRE types: genes linked to *de novo* and increasing promoters were largely upregulated, while those associated with decreasing promoters showed consistent downregulation (ANOVA with Tukey's honestly significant difference [HSD] test, $p < 0.05$) (Figure 3B). The target genes of *de novo* and increasing enhancers displayed no statistically significant differences between them, but differed significantly from those associated with decreasing enhancers across all time points (Figure 3B). Furthermore, the target genes of *de novo* and increasing RREs

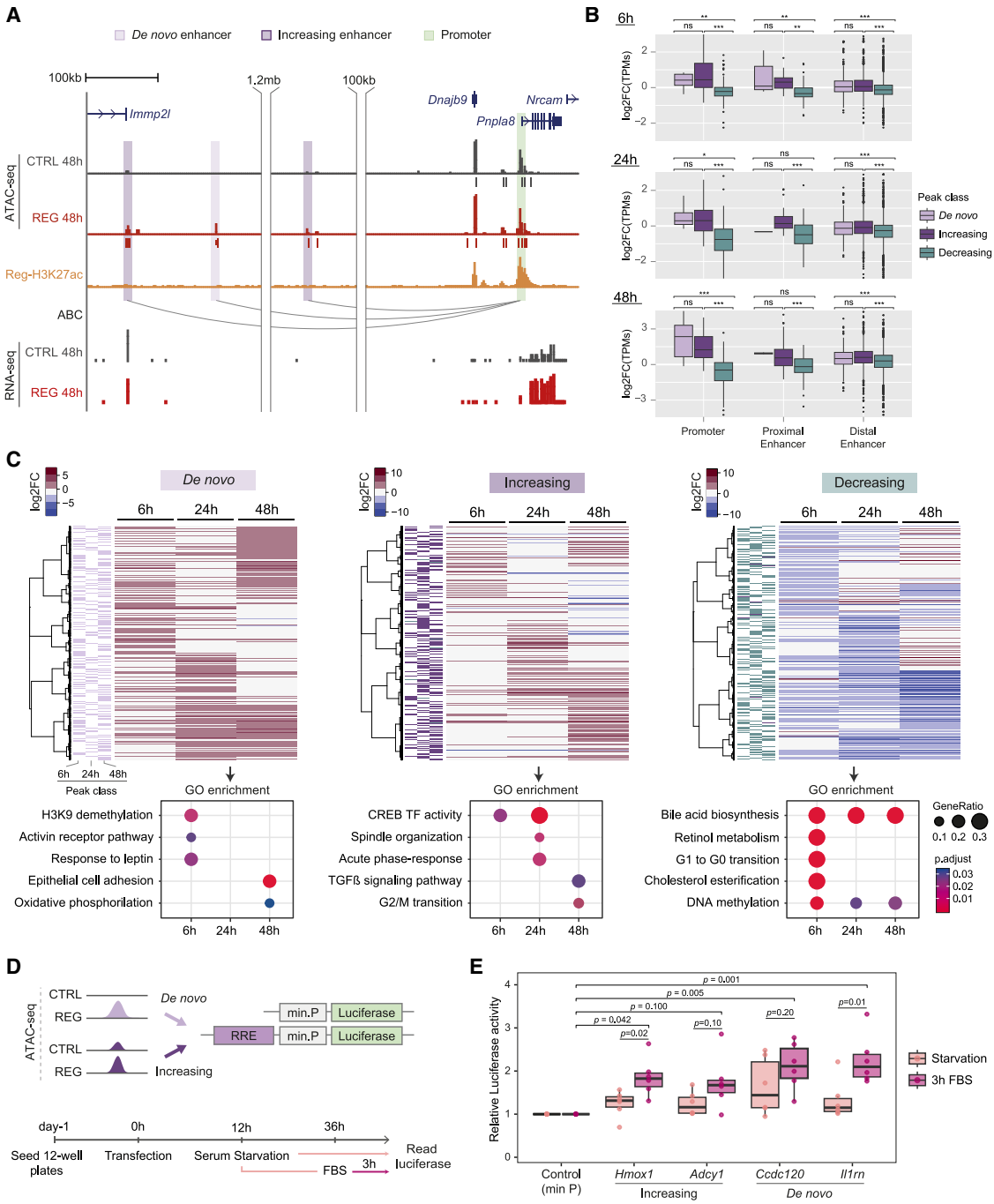

Figure 3. Enhancer-gene predictions using the ABC algorithm reveal opposite regulation for proliferation and metabolic genes

(A) Genome browser screenshot showing an ABC algorithm prediction at 48 h post-PHx. One *de novo* and two increasing enhancers (light and dark purple) are linked to the upregulated gene *Pnpla8*, located kilobases away. One replicate is shown for simplicity.

(B) Log2FC (TPM) of target genes associated with RREs in REG vs. CTRL samples. Two-way ANOVA followed by Tukey's HSD test was used to assess statistical differences between peak classes (*de novo*, increasing, and decreasing) and genomic regions (promoter, proximal, distal) at 6, 24, and 48 h. Significance shown only between peak classes: ns, non-significant; $^{*}p_{adjusted} < 0.05$, $^{**}p_{adjusted} < 0.01$, $^{***}p_{adjusted} < 0.001$.

(C) Expression of target genes linked to *de novo*, increasing, and decreasing RREs, clustered by log2FC (TPM), gene order was established by hierarchical clustering. (Below) Time-specific GO terms enriched in each RRE class (one-sided Fisher's exact test $p_{adjusted} < 0.05$).

(legend continued on next page)

tended to be upregulated during regeneration, whereas decreasing RREs were found to be mainly associated with downregulated genes (Figure 3C). GO analysis revealed that *de novo* and increasing RRE target genes were significantly enriched in signaling pathways known to play a role in liver regeneration at all three time points, such as the activin/TGF-β pathway,[19] with increasing RREs also associated with genes involved in the cell cycle (Figure 3C). In contrast, decreasing RREs mainly controlled the expression of genes related to liver-specific functions in lipid metabolism, including pathways associated with cholesterol and retinol metabolism, as well as bile acid biosynthesis. These findings align with the enriched biological functions identified in our transcriptomics analysis. Notably, the target genes from *de novo* and increasing RREs were enriched in functions that parallel those of the REG-specific transcriptomic gene clusters (Figure 1D), including the acute-phase response at 24 h and the mitosis-related signaling pathways at 48 h post PHx. In contrast, the steroids/cholesterol, retinol and bile acid metabolic pathways, specifically enriched for decreasing RRE-target genes, also exhibited enrichment within the cluster of control-specific genes from the RNA-seq analysis (Figure 1D). This suggests that *de novo* and increasing enhancers are activated post PHx to upregulate genes required for early liver regeneration, whereas decreasing RREs influence gene expression in the intact adult liver but have reduced activity after PHx. Furthermore, our analysis revealed an enrichment of genes associated with the DNA methylation pathway among all decreasing RREs (Figure 3C). The dynamics of DNA methylation during liver regeneration are complex,[45] and consistent with this, we identified genes within this group involved in both methylation and demethylation processes.

To validate putative RREs as enhancers capable of driving gene expression, we conducted a transient reporter assay in hepatocyte cell cultures. We cloned candidate RREs upstream of a minimal promoter and a luciferase gene cassette to assess their enhancer activity. Specifically, we tested four candidate sequences: (1) a distal increasing enhancer upstream of *Hmox1*; (2) an increasing enhancer located within the 10th intron of *Adcy1*; (3) a proximal *de novo* enhancer that progressively gains accessibility and is predicted to regulate *Ccdc120*, a gene exhibiting increased expression throughout regeneration; and (4) an intronic *de novo* enhancer predicted by the ABC model to target *Il1rn*, a gene upregulated 6 h post PHx (Figure S3C). These constructs were transiently transfected into a hepatocyte cell line,[46] serum starved for 24 h to induce quiescence, and then either stimulated with 10% fetal bovine serum for 3 h or maintained in serum-free conditions (Figure 3D), mimicking the quiescence-to-proliferation transition characteristic of liver regeneration. Serum stimulation significantly increased luciferase activity for the *Hmox1* (increasing) and *Il1rn* (*de novo*) RREs ($n = 6$, ANOVA with Tukey's HSD test, $p < 0.05$), while the other two showed non-significant increases (Figure 3E). Under serum conditions, all four RREs exhibited significantly higher activity than the control, but not under starvation, suggesting that they act as enhancers activated upon cell cycle re-entry.

Cascade of TF activation during early liver regeneration

We next conducted a TF footprint analysis within RREs using HINT-ATAC[47] to identify potential transcriptional regulators of the liver response after PHx. We identified differential TF footprints by comparing the ATAC-seq profiles of regenerating and control livers within all RREs at each time point. Only TFs that were expressed in our transcriptomics data and exhibited a significant change in activity ($p < 0.05$) were considered in the analysis.

We observed that predicted TFs footprints within RREs during liver regeneration differed entirely from those in control livers (Figure 4A). Across all regeneration time points, we identified various combinations of the activator protein-1 (AP-1) dimer motif (FOS/JUN) (Figure S4A) and the nuclear factor erythroid 2 (NFE2) binding site. Some motifs were shared between two time points, such as early growth response 2 (EGR2) at 6 and 48 h, and CCAAT/enhancer-binding protein β (C/EBPβ) at 24 and 48 h post PHx. Others were exclusive to specific time points, including EGR1 and MYC at 6 h; and activating TFs (ATFs) 1, 3 and 7, NFE2-related factor 2 (NRF2), X-box binding protein 1 (XBP1), and One-cut1/hepatocyte nuclear factor 6 at 24 h (Figures 4A and S4B–S4E). At 48 h, we detected Mothers against decapentaplegic homolog 3 (SMAD3) footprints (Figure 4A), and although not significantly, the NRF2 motif also seemed to be enriched (Figure S4E). Notably, many of these TFs were upregulated at the transcriptional level, including *Fos*, *Jun*, *Egr1*, *Atf3*, *Nrf2*, and *Cebpβ* (Figure 4B). Several of these are well-known regulators of the transcriptional response during liver regeneration. For instance, *Fos* and *Jun* are immediate-early genes induced within the first hours after PHx, playing a key role in promoting hepatocyte proliferation.[19] Similarly, C/EBPβ contributes to cytokine-mediated activation pathways and supports both proliferation and metabolic homeostasis in remnant hepatocytes,[17] while XBP1 regulates proteostasis and the acute-phase response during liver regeneration.[48] In control livers, we predicted the binding sites for D-box binding PAR bZIP TF (DBP) and C/EBPα (Figure 4A), both of which showed decreased expression at 48 h after PHx (Figure 4B), along with nuclear factor interleukin 3 regulated (NFIL3), among others.

To further investigate putative TFs involved in liver regeneration, we analyzed motif enrichment in RREs using AME (MEME Suite).[49] We compared TF motif enrichment in *de novo* and increasing or decreasing RREs at each time point against all accessible regions (Mann-Whitney U test $p < .05$). Since the motifs within enhancer and core-promoter sequences may recruit different *trans*-acting factors,[50] we analyzed them separately. We selected the top 10 TF motifs per time point and peak class,

(D) Reporter assay design. Candidate *de novo* and increasing RREs were cloned upstream of a luciferase cassette, transfected into hepatocyte cultures, serum-starved for 24 h, then either kept in starvation or treated with 10% fetal bovine serum (FBS) for 3 h. The constructs were measured in two independent experiments in a total of six biological replicates.

(E) Relative luciferase activity under starvation or FBS treatment. Two-way ANOVA with Tukey's HSD test was used to compare constructs vs. minP and between serum conditions ($p < 0.05$). See also Figure S3.

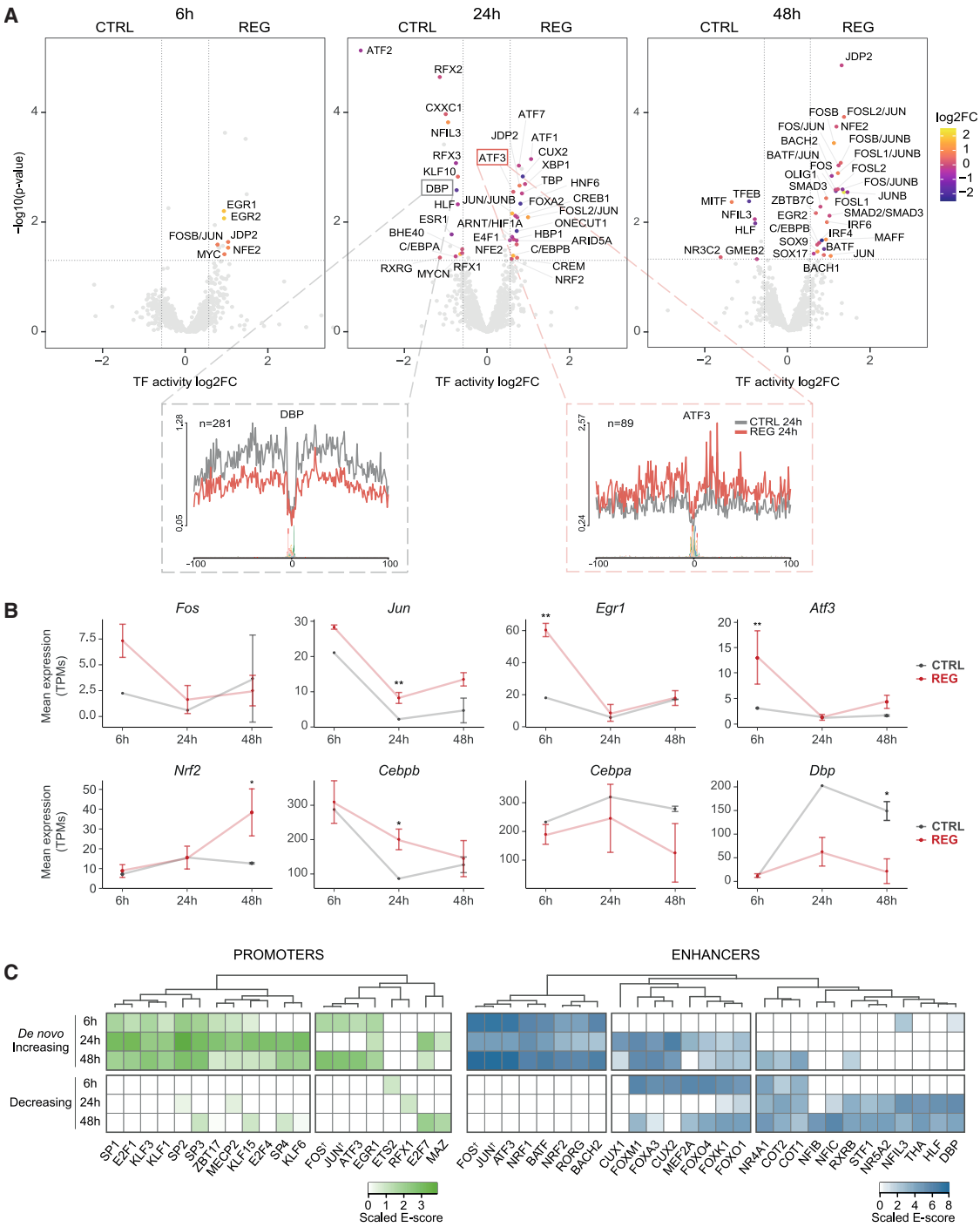

Figure 4. Time point-specific TF motif patterns during liver regeneration

(A) Differential TF binding sites at each time point identified by HINT-ATAC[47] footprinting. Each point represents a TF; only those with expression >1 TPM in at least one condition and significant change in activity ($p < 0.05$) are labeled. Circle color reflects log2FC of the TF-encoding gene. (Below) ATAC-seq profiles for two example TF footprints at 24 h post PHx (CTRL vs. REG).

(B) Expression of *Fos*, *Jun*, *Egr1*, *Atf3*, *Nrf2*, *Cebpb*, *Cebpa*, and *Dbp* over time in CTRL (gray) and REG (red). Significance: $^{**}p_{adjusted} < 0.01$, $^{*}p_{adjusted} < 0.05$ (DESeq2, pairwise comparison vs. control, Wald test, assuming negative binomial distribution).

(C) Top 10 enriched TF motifs in *de novo*, increasing, or decreasing promoters (left) and enhancers (right), identified using AME[49] with the HOCOMOCO v11 database (Mann-Whitney U test, $p_{adjusted} < 0.05$). Scaled enrichment E-scores are shown. †Includes all family members. See also Figure S4.

excluding non-expressed TFs. Our analysis revealed substantial differences between promoters and enhancers, and distinct TF motif patterns in increasing or decreasing regions (Figure 4C). E2F, SP, and Krüppel-like factor motifs were consistently enriched in *de novo* and increasing promoters across all time points, with several encoded by genes co-expressed in the 6 or 6–48 h REG clusters (Table S1). The E2F family is known for its critical role in regulating the cell cycle and apoptosis, with E2F1 specifically binding to the promoter regions of genes involved in the progression to the S phase.[51] FOS and JUN motifs were also among the top hits, enriched in both *de novo* and increasing promoters and enhancers, but absent from decreasing RREs (Figure 4C). These TFs were highly expressed in the liver at 6 h post PHx (Figure 4B). We also identified the STAT3 motif, a key TF driving hepatocyte proliferation during liver regeneration,[52] exclusively enriched in *de novo* and increasing enhancers at both 6 h ($p_{adjusted} = 4.23e^{-04}$) and 48 h ($p_{adjusted} = 2.11e^{-07}$) post PHx (Figure S4F). Although STAT3 was not among the top 10 enriched motifs, its significant enrichment, along with the strong enrichment for the E2F and AP-1 motifs, further supports the robustness of our findings. In addition, the ATF3 motif was enriched in both *de novo* and increasing promoters and enhancers, with NRF1 and NRF2 motifs also exclusively enriched within these enhancers. In contrast, decreasing enhancers showed enrichment for the COUP TFs 1 and 2, nuclear factors I (NFI) B and C, and DBP motifs (Figure 4C).

Subsequently, we integrated our transcriptomics data, TF binding predictions, and enhancer-gene map to construct a GRN. We selected the top 10 most enriched TFs in RREs at each time point (Figure 4C) and computed Pearson's correlation coefficients between the expression of each TF and that of its predicted target genes. We retained only significant interactions ($|correlation| \geq 0.8$) and TFs with motifs present in at least five RREs. Most TFs showed positive correlations with their targets, suggesting a predominantly activating role via enhancers (Figures 5A, S5A, and S5B). For instance, NRF2 positively correlated with all its targets, especially at later stages, whereas BACH2 showed mixed effects, negatively correlating with 66% of its targets (Figures S5A–S5C).

We next profiled gene expression over time and categorized edges based on their corresponding RRE behavior at each time point. The resulting GRN suggested a cascade of TF activation during the early stages of liver regeneration (Figures 5B–5D). At 6 h post PHx, key early induced TFs, including EGR1, the AP-1 subunits JUN and FOS, and ATF3, were upregulated, likely driving the expression of their target genes via *de novo* and increasing enhancers (Figures 5B–5F and S5D). As regeneration progressed, additional TFs, such as CUX1, may have contributed to the transcriptional activation of genes at 24 h (Figure 5C). By 48 h after PHx, several TFs including NRF2, FOXM1, MEF2A, NRF1, and FOXK1 emerged as potential central drivers of gene upregulation (Figures 5D, S5D, and S5E). Notably, we observed co-localization of NRF2 and FOXM1 motifs at numerous RREs, suggesting potential cooperation in activating their target genes at 48 h post PHx (Figures 5G, 5H, and S5F). Conversely, some TFs likely mediated the downregulation of their target genes at specific time points. For instance, FOXK1, FOXO4, and FOXM1 motifs were primarily associated with decreasing enhancers and low gene expression at 6 h post PHx (Figures 5B and S5D). Meanwhile, downregulated regulons at 24 and 48 h included DBP, NFIB, and NFIC (Figures 5C, 5D, S5D, and S5E).

Focusing on ATF3, which was significantly upregulated at 6 h post PHx (Figure 4B), we performed immunohistochemical analysis and confirmed the presence of ATF3-positive hepatocyte nuclei in regenerating livers at this time point, but not in controls (Figure 6A). Next, we identified a set of putative ATF3 target regions by analyzing available ATF3 ChIP-seq datasets in mice and comparing them with *de novo* and increasing RREs. ATF3 peaks were significantly enriched at these RREs, particularly at 6 h post PHx (Fisher's exact test, $p_{adjusted} < 0.001$) (Figure 6B), supporting the GRN predictions. Further analysis confirmed that ATF3 binds to the promoters and enhancers of over 85% of the GRN-predicted ATF3 target genes. Among these, *Hcar2*, which was upregulated at 6 h, was associated with a *de novo* RRE (Figure 6C), while *Trib1,* previously shown to be regulated by ATF3 in HepG2 cells,[53] was linked to three increasing enhancers with ATF3 binding (Figure S6A). Additionally, functional characterisation of predicted ATF3 target genes linked to *de novo* and increasing RREs (Table S4), using the Kyoto Encyclopedia of Genes and Genomes Pathway database, revealed enrichment in regeneration-related pathways. These included glucagon signaling and adherens junctions across all time points, as well as the MAPK, TGF-β, and Hippo signaling pathways, particularly at later stages (Figure 6D). Furthermore, we analyzed *Atf3* expression using a published single-cell RNA-seq dataset from livers collected at different time points post PHx,[31] although no scRNA-seq data were available for 6 h. *Atf3* was predominantly expressed in a subset of hepatocytes at 24 and 48 h post PHx (Figures 6E and 6F), confirming that its expression was mostly restricted to regenerating hepatocytes. Moreover, GRN-predicted ATF3 target genes, validated through ChIP-seq analysis, exhibited higher expression levels in *Atf3*-expressing cells compared with those without *Atf3* expression (Figure S6B). Altogether, these findings support our GRN predictions and highlight the role of ATF3 in transcriptional regulation during liver regeneration.

We next integrated our ATAC-seq dataset with the published NRF2 ChIP-seq profiles from mouse intact livers.[54] NRF2 is a TF that plays a key role in the response to oxidative stress by binding to the antioxidant response elements in the promoter regions of cytoprotective genes, such as phase II detoxification enzymes, thus inducing their expression.[55] We focused our analysis on increasing RREs, since these regions were more likely to feature NRF2 in the intact liver. Indeed, we observed a significant overlap between increasing RREs and NRF2 peaks at all time points (Fisher's exact test, $p_{adjusted} < 0.001$), with this overlap becoming more pronounced at the later stages of regeneration (Figure 6G). These results are consistent with the concurrent increase in *Nrf2* expression over time (Figure 4B) and further reinforce the role of NRF2 especially at this later time point. *Hmox1*, a well-established NRF2 target,[56] was upregulated 48 h post PHx and associated with an NRF2-bound increasing RRE (Figure 6H). Similarly, *Aldh1a7*[57] was also upregulated and linked to an NRF2-bound increasing RRE (Figure 6H). Moreover, single-cell analysis of *Nrf2* expression[31] revealed its overexpression in

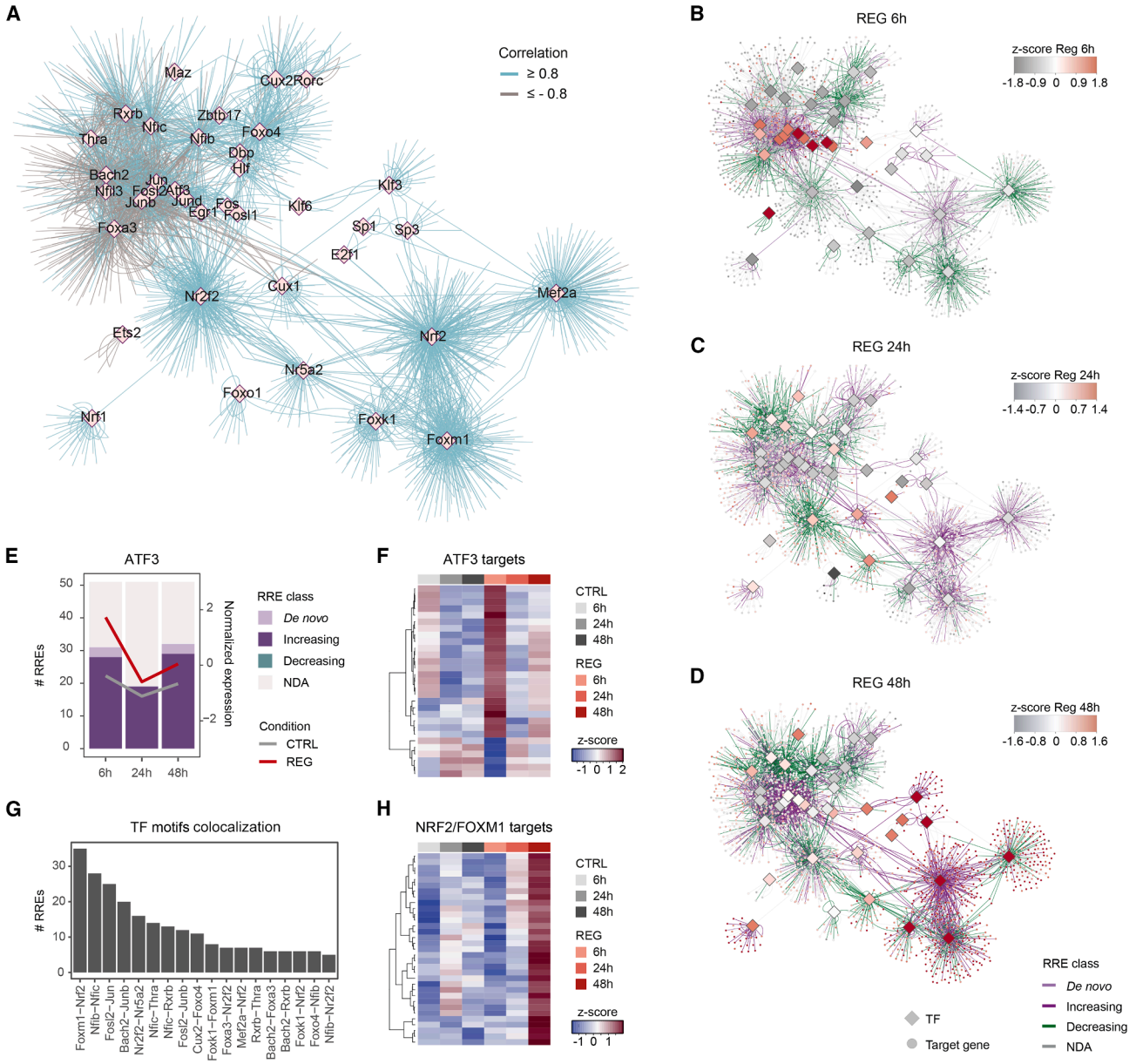

Figure 5. Early regeneration GRN

(A) GRN with edges colored by TF-target Pearson's correlation coefficient (blue, $\geq$0.8; gray, ≤ -0.8). While most correlations are positive, negative interactions are predicted for some TFs.

(B) GRN at 6 h: Nodes are colored by target gene normalized expression and edges by RRE classification at 6 h.

(C) GRN at 24 h: same as (B), but for 24 h.

(D) GRN at 48 h: same as (B), but for 48 h.

(E) Number and type of RREs with ATF3 motifs (left axis) and *Atf3* expression in *Z* scores (right axis) (REG in red, CTRL in gray).

(F) Expression of predicted target genes linked to ATF3 motif-containing RREs. Each column is one condition (average across replicates), gene expression as *Z* scores.

(G) Number of RREs containing TF motif pairs.

(H) Expression of predicted target genes associated with RREs with co-localization of the NRF2 and FOXM1 motifs. Each column is one condition (average across replicates), gene expression as *Z* scores. See also Figure S5.

hepatocytes at 24 and 48 h post PHx (Figure S6C), with a similar expression pattern observed for its known target genes, *Hmox1* and *Aldh1a7* (Figures S6D and S6E). Overall, NRF2 target genes, identified by the GRN and validated by ChIP-seq, showed significantly higher expression in *Nrf2*-expressing cells compared with non-expressing ones in the scRNA-seq data (Figure S6B).

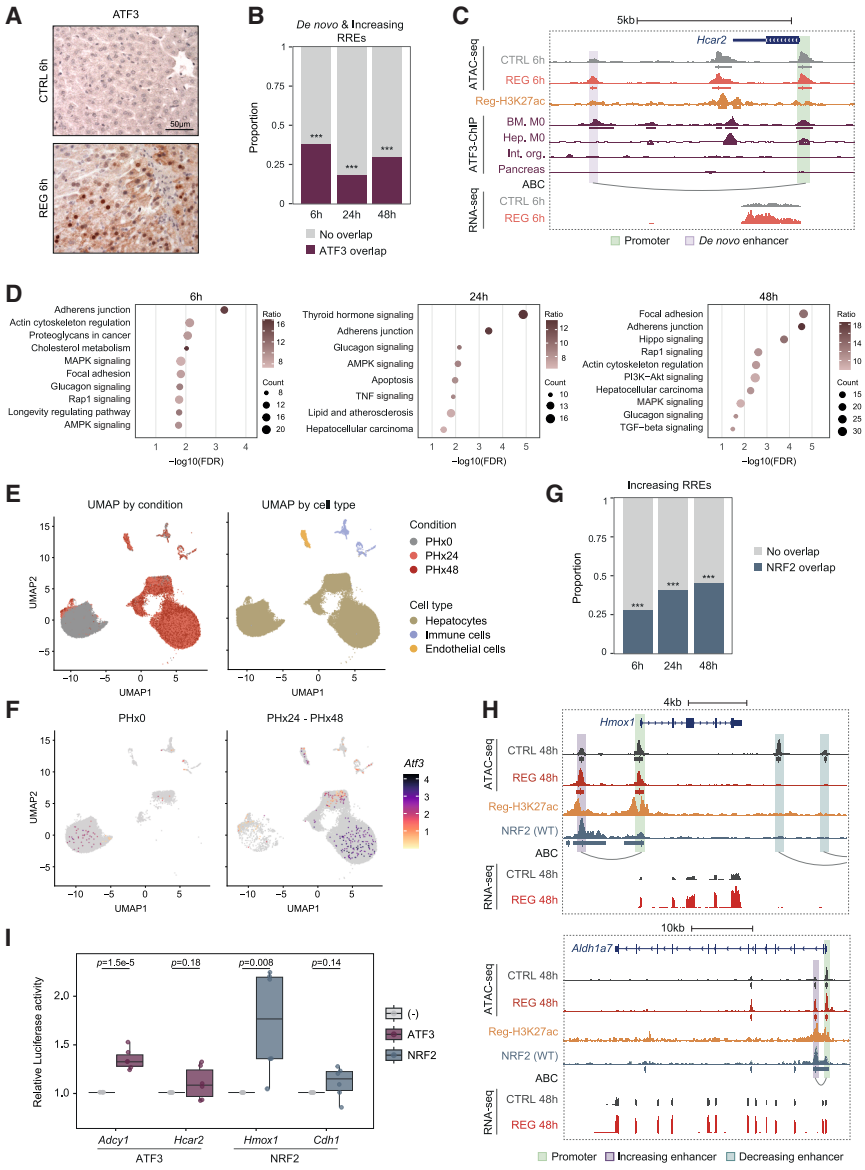

Figure 6. ATF3 and NRF2 bind to *de novo* and increasing RREs to activate the expression of regeneration-associated genes

(A) Representative ATF3 immunostaining images in control and regenerating livers at 6 h post surgery. No positive nuclei observed in controls.

(B) Proportion of *de novo* and increasing RREs overlapping ATF3 ChIP-seq peaks at each time point. Fisher's exact test (***$p_{adjusted} < 0.001$).

(C) Genome browser screenshot of the *Hcar2* locus at 6h. Promoter shows ATF3 binding and is linked to an ATF3-bound *de novo* enhancer.

(D) Kyoto Encyclopedia of Genes and Genomes (KEGG) Pathway analysis of target genes from ATF3-bound *de novo* and increasing RREs ($p_{adjusted} < 0.05$).

(E) UMAP of cells from quiescent (PHx0) and regenerating (PHx24–PHx48) livers, colored by condition (left) or annotated cell type (right).

(F) Feature plot of *Atf3* expression at PHx0 and PHx24–PHx48.

(G) Proportion of increasing RREs overlapping NRF2 ChIP-seq peaks at each time point. Fisher's exact test (***$p_{adjusted} < 0.001$).

(H) Genome browser views of *Hmox1* and *Aldh1a7* loci at 48 h. Both promoters show NRF2 binding and are linked to NRF2-bound increasing enhancers.

(I) Relative luciferase activity of candidate enhancers co-transfected with ATF3 or NRF2 vectors, or alone (−), in hepatocyte cultures. One-way ANOVA with Tukey's HSD ($p < 0.05$). See also Figure S6.

Functional analysis of NRF2-bound increasing RRE targets revealed enrichment in wound healing, kinase activity, apoptosis, angiogenesis, and epithelial proliferation (Figure S6F; Table S5). As expected, when all target genes were considered, there was enrichment for oxidative stress response (GO: 0006979; $p_{adjusted} = 2.10e^{-03}$). This suggests NRF2 may bind both promoters and enhancers of regeneration-related genes under normal conditions, but during regeneration increased *Nrf2* expression and RRE accessibility likely promote NRF2 binding to RREs, leading to target gene upregulation. In contrast, DBP, which is downregulated during regeneration according to our transcriptomics analysis (Figure 4B) and the published scRNA-seq data[31] (Figure S6G), likely detaches from RREs, contributing to their closure and reduced gene expression.

To confirm that ATF3 and NRF2 act as transcriptional activators of liver regeneration through RREs, we co-transfected expression vectors for these TFs with luciferase reporter vectors containing candidate enhancers. For ATF3, we tested RREs associated with *Hcar2* (Figure 6C) and *Adcy1* (Figure S3C), both identified by the GRN as ATF3 targets. As candidate NRF2-regulated enhancers, we selected the *Hmox1*-linked enhancer (Figure 6I) and an intronic enhancer associated with *Cdh1*, a gene upregulated at 48 h post PHx and predicted by the GRN as a potential NRF2 target. Transient co-transfection assays in hepatocyte cultures revealed a significant increase in luciferase expression in ATF3-expressing cells with the *Adcy1*-associated RRE and in NRF2-expressing cells with the *Hmox1* RRE, compared with non-expressing control cells (-ANOVA with Tukey's HSD; $p < 0.05$) (Figure 6I). Additionally, the *Hcar2* and *Cdh1* enhancers showed a trend toward increased luciferase activity upon ATF3 and NRF2 overexpression, respectively. These results support ATF3 and NRF2 as transcriptional activators of RREs.

Interplay of regeneration-specific and developmental regulatory elements

While liver regeneration and development share some molecular mechanisms, the two processes differ significantly. For instance, their cellular origins are distinct: liver regeneration after

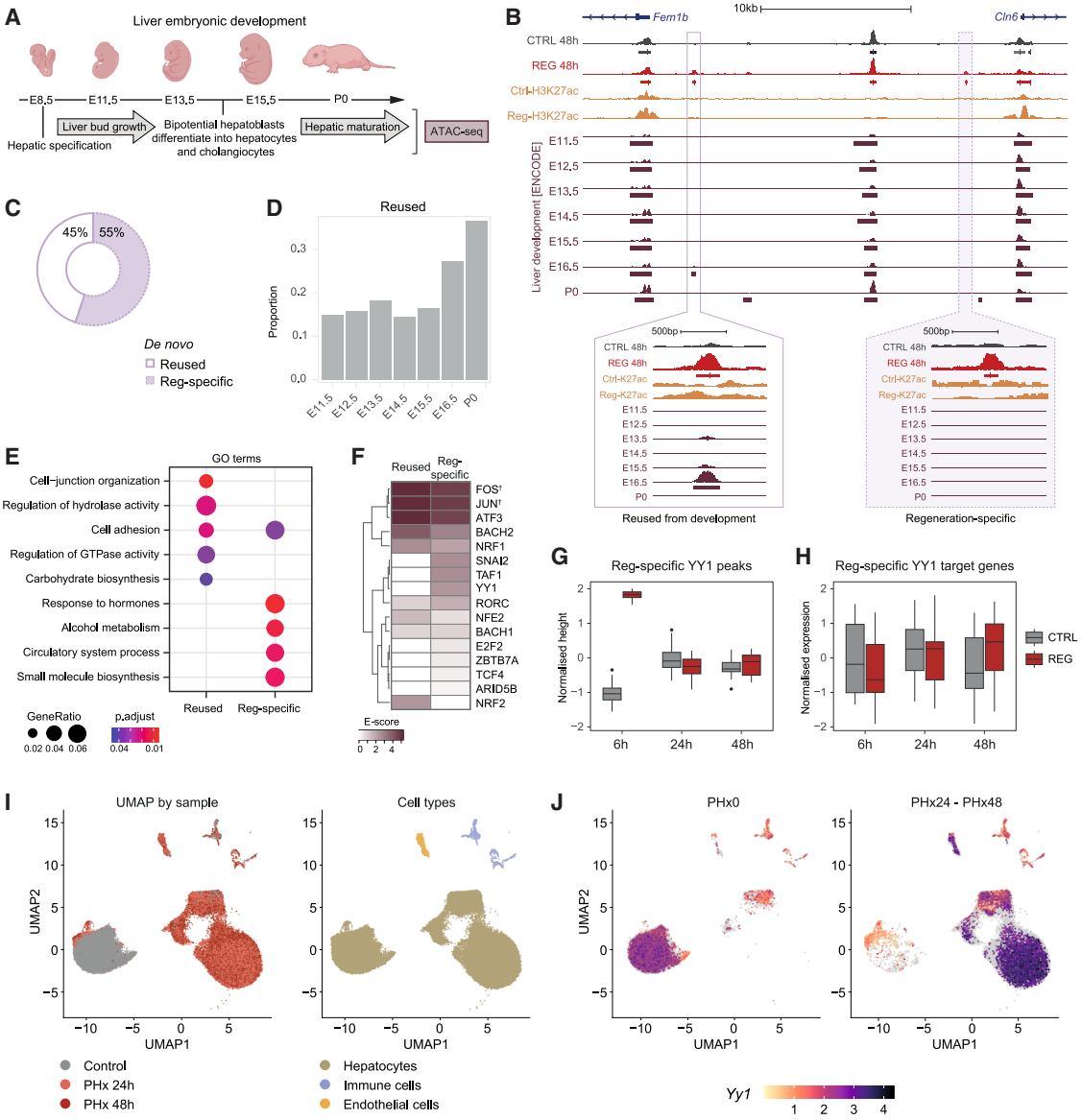

Figure 7. Enhancers from development are repurposed in the adult liver to activate the expression of regeneration genes

(A) Liver developmental stages used for ATAC-seq data in the comparative analysis with *de novo* RREs.

(B) Genome browser views of a *de novo* enhancer overlapping a developmental enhancer (Reused) and one specific to regeneration (REG specific).

(C) Proportion of *de novo* RREs classified as reused or REG specific.

(D) Proportion of *de novo* peaks overlapping developmental enhancers at each developmental stage.

(E) GO term analysis of target genes from reused vs. REG-specific *de novo* RREs ($p_{adjusted} < 0.05$).

(F) Heatmap of enriched TF motifs in reused and REG-specific *de novo* RREs. Scaled enrichment E-score shown. †All family members included.

(G) Normalized accessibility of REG-specific *de novo* peaks with YY1 motifs.

(H) Normalized expression of REG-specific YY1 putative target genes.

(I) UMAP of gene expression from quiescent (PHx0) and regenerating livers (PHx24, PHx48), colored by condition (left) and annotated cell type (right).

(J) Feature plot of *Yy1* expression in PHx0 and PHx24-PHx48. See also Figure S7.

PHx is primarily driven by mature hepatocytes, whereas during embryonic development, hepatocytes originate from hepatoblasts—bipotential precursors that also give rise to biliary epithelial cells.[19] To determine if the gene expression changes observed during liver regeneration rely on the same regulatory mechanisms used during liver development or involve unique, regeneration-specific regulatory networks, we analyzed chromatin accessibility data from mouse liver development, spanning embryonic day 11.5 (E11.5) to postnatal day 0 (P0)[58] (Figure 7A). This period encompasses the stages of accelerated liver bud growth (E10–E13), hepatoblast differentiation into hepatocytes (E14), and hepatocyte maturation (E15–P0), a process

that continues after birth.[19] We specifically examined whether *de novo* RREs—regions uniquely accessible in regenerating livers but not in uninjured ones—were also accessible during any stage of liver development. Such overlap would indicate the reuse of developmental enhancers for regeneration. Conversely, regions exclusively accessible during regeneration, with no accessibility during development, would suggest the presence of regeneration-specific enhancers (Figure 7B). Our analysis revealed that 45% of *de novo* RREs were developmental enhancers repurposed for regeneration (Reused), while the remaining 55% were enhancers exclusive to regeneration (REG specific) (Figure 7C). Among the Reused enhancers, most were either repurposed from late developmental stages (E16.5 and P0) (Figures 7B–7D) or were active throughout all stages of liver development (Figures S7A and S7B). To further characterize these regulatory elements, we explored their distribution in the genome. While both subtypes of *de novo* RREs were predominantly located in distal regions, consistent with the general distribution of all RREs, their proportions in proximal and promoter regions differed significantly (chi-square $p < 2.2e{-}16$). Specifically, Reused RREs were more abundant in proximal (2%) and promoter (6%) regions, compared with REG-specific regulatory elements (1% and 2%, respectively). These findings suggest that regeneration-specific regulatory mechanisms primarily function through distal enhancers.

GO term enrichment analysis of *de novo* RRE target genes revealed distinct functional categories. Reused RRE genes were enriched in cell-cell interactions and carbohydrate biosynthesis, including gluconeogenesis genes like *Sik1* (Figures 7E and S7C), a process regulated during both regeneration and birth.[59] In contrast, REG-specific targets were enriched in liver-related functions, such as alcohol metabolism and hormone responses, including insulin, leptin, and growth hormone signaling, such as peroxisome proliferator-activated receptor gamma (*Pparg*) gene (Figures 7E, S7D, and S7E). These pathways act as auxiliary mitogens, delaying but not impairing regeneration when disrupted.[18]

Next, we performed TF motif enrichment between REG-specific and Reused *de novo* RREs (Figure 7F). Although many TFs were shared between these two groups, distinct TF signatures were identified. For instance, NRF2 was exclusively enriched in Reused enhancers, while other TFs, such as the transcriptional repressor YY1, were uniquely enriched in REG-specific enhancers. We focused on YY1 due to its well-established role in intestinal stem cell renewal[60] and its involvement in hepatic lipid metabolism.[61] YY1 overexpression promotes the growth of immortalized, non-tumorigenic human hepatocytes, whereas its depletion inhibits the growth of hepatocellular carcinoma cells.[62] We observed that the YY1 binding motif was predominantly enriched in REG-specific *de novo* RREs that became accessible at 6 h after PHx (Figure 7G), while its predicted target genes were generally downregulated at this time point (Figure 7H). Pearson's correlation coefficient analysis between the accessibility of these REG-specific RREs with YY1 motifs and the expression of their associated target genes revealed that nearly 70% exhibited a negative correlation (Figure S7F). This suggests that these regions might function as REG-specific silencers rather than enhancers, consistent with the role of YY1 as a transcriptional repressor.[63] To determine which cells express *Yy1* during regeneration, we analyzed a published scRNA-seq dataset from livers collected at 0, 24, and 48 h post-PHx.[31] We found that *Yy1* was highly expressed in hepatocytes and endothelial cells during regeneration, with lower levels of expression observed in quiescent hepatocytes and immune cells (Figures 7I and 7J). Altogether, our results suggest that liver regeneration involves a collaborative interplay between regeneration-specific regulatory elements and developmental enhancers repurposed in adulthood, each governed by distinct regulatory mechanisms and linked to specific biological functions.

DISCUSSION

The mammalian liver possesses an exceptional capacity for compensatory growth following injury or PHx, a process driven by transcriptional reprogramming and epigenetic modifications.[21,24] In quiescent hepatocytes, pro-regenerative genes are maintained in active or permissive chromatin states,[27,64] enabling rapid and widespread transcriptional changes in response to injury.[65] During regeneration, some hepatocytes preserve their original chromatin landscape, while others shift toward a fetal-like state.[30,31] Despite significant progress in understanding the epigenetic events of liver regeneration, the mechanisms regulating chromatin architecture, specific enhancers, and transcriptional networks that control regenerative programs remain unclear.

Here, we identify the regulatory elements that are dynamically modulated during early liver regeneration after PHx (RREs) and uncover new TFs potentially regulating their activity. RREs mainly function as enhancers activating the expression of regeneration-associated genes, particularly those involved in key signaling and cell cycle pathways. However, RREs also include regions that become inactive during regeneration, which may lead to a global downregulation of liver-specific homeostatic functions, such as the biosynthesis of bile acids and retinol. This suggests that hepatocytes suppress energy-intensive metabolic programs characteristic of quiescent hepatocytes to prioritize proliferation. An inverse correlation between hepatocyte proliferation and metabolic function during liver regeneration has been previously proposed.[65,66] A similar shift in chromatin accessibility has been observed in chronic liver injury,[28] and spatially resolved transcriptomics during liver regeneration further confirm an initial downregulation of metabolic genes, concurrent with hepatocyte priming and proliferation.[32] Consistently, single-cell studies show that regenerating hepatocytes undergo reprogramming after PHx, shifting from metabolic to developmental functions.[30,31] However, a subset of hepatocytes retains the chromatin landscape of metabolically active uninjured cells.[30,31] Consequently, changes in RRE accessibility may occur selectively within specific hepatocyte populations.

Hepatocyte metabolic reprogramming in the injured liver is essential for meeting energy demands, supplying anabolic precursors, and regulating signaling pathways that drive tissue repair.[67] Our findings suggest that, during regeneration, hepatocytes suppress bile acid biosynthesis and undergo changes in cholesterol metabolism through transcriptional and chromatin regulation. While lipid utilization increases during regeneration

to support the synthesis of phospholipids and cholesterol, both essential for cell membrane formation,[68] repression of *Cyp7a1* post PHx limits bile acid production from cholesterol, despite Cyp7a1 protein levels remaining stable.[36,69] Furthermore, the ubiquitin ligase Uhrf2-mediated suppression of cholesterol biosynthesis genes is essential for regeneration,[70] and a hypercholesterolemic diet impairs liver repair.[71] Further studies are warranted to elucidate the relationship between steroid metabolic regulation and hepatic regeneration.

Our study also identifies potential transcriptional regulators orchestrating liver regeneration. The AP-1 complex emerges as a key factor driving the transcriptional response at the chromatin level, especially during the priming phase. In particular, the AP-1 subunit JUN is a critical regulator of hepatocyte proliferation, as studies have shown that liver regeneration is impaired in mice lacking JUN.[72] The role of AP-1 appears to be conserved across various regenerative models,[73] including *Drosophila* wing discs[8] and zebrafish heart,[74] as well as killifish and zebrafish fin regeneration,[6] in which AP-1 motifs are essential for the activation of RREs. Consequently, the AP-1 complex may serve as a master regulator, collaborating with tissue-specific TFs, to facilitate the opening of *de novo* RREs as a pioneer factor and activate gene expression during regeneration. Significantly, recent evidence suggests that AP-1 can act as a pioneer factor in hepatocytes by contributing to global changes in chromatin accessibility after *in vivo* reprogramming by the Yamanaka factors.[75] Furthermore, our findings suggest a cascade of TF activation after PHx, with ATF3, alongside JUN and FOS, driving the transcriptional response during the priming stage of liver regeneration. While the role of ATF3 in liver regeneration remains unclear, it is rapidly induced after PHx in rats[76] and has been implicated in various processes, including hepatic proliferation,[77] the inhibition of gluconeogenesis,[78] a liver-specific function that is initially downregulated during liver regeneration,[79] and the regulation of lipoprotein and bile acid metabolism,[80] processes that undergo alterations during liver regeneration, as observed in our study. Here, we propose that ATF3 selectively binds to the promoters and enhancers of genes essential for the initiation of regeneration, while NRF2 and FOXM1 likely mediate gene upregulation during the proliferation stage. Significantly, it has been demonstrated that the absence of NRF2 impairs liver regeneration,[81] while its ectopic activation enhances regenerative capacity.[82] Moreover, previous studies have shown that FOXM1 is essential for hepatocyte mitosis by stimulating the expression of cell cycle genes during liver regeneration.[83]

A long-standing question in regenerative biology is whether regeneration recapitulates embryonic development. Research in animals with a high regenerative potential has shown that the genes involved in development are frequently reactivated after injury and are essential for successful regeneration.[84,85] However, evidence also suggests that the regulatory networks controlling tissue regeneration and proliferation in wounded tissues differ from those involved in developmental growth.[1] In the liver, recent studies indicate that a subset of hepatocytes undergo reversible reprogramming after PHx, activating the same gene expression programs that are used for physiological growth during the postnatal stage of development.[30,31] At the same time, STAT3 binding to injury-specific enhancers, rather than developmental enhancers, to activate reprogramming-related genes[86] suggests distinct regulatory networks between regeneration and development. Our findings indicate that the regenerating liver is capable of reactivating developmental enhancers, preferentially from the postnatal or late developmental stages, to regulate genes associated with cell junctions and glucose metabolism. Significantly, hepatocytes acquire junctional integrity and polarity and undergo changes in glucose metabolism during the maturation stage of liver development, a process that takes place around the perinatal period.[19] These changes bear resemblance to those observed during liver regeneration after PHx.

In summary, our study provides a genome-wide atlas of enhancer-gene interactions and highlights key transcriptional regulators in early liver regeneration. These findings could be a valuable resource for researchers aiming to target regulatory elements involved in liver regeneration, with significant implications for regenerative medicine. Potential applications include the ectopic activation of regeneration enhancers to exert temporal and spatial control over the expression of pro-regenerative factors within an injured area, as proposed by Yan et al.[16] The addition of regenerative TFs could also be used to enhance the regenerative potential, particularly in the context of liver failure.

Limitations of the study

While this study provides key insights into liver regeneration, more biological replicates would improve robustness, and additional time points could provide a more comprehensive understanding of the process. *In vivo* transgenic reporter assays could further clarify enhancer function during regeneration. However, compliance with stringent European regulations on animal research limits the inclusion of additional replicates, time points or transgenic models. Future studies could also benefit from experiments such as ChIP-seq for TFs identified in our GRN. The lack of high-quality antibodies, particularly for TFs with less characterized roles in liver regeneration, has limited our ability to generate ChIP-seq data using liver tissue from hepatectomies. The absence of detectable changes in chromatin accessibility does not necessarily indicate that specific enhancers or regulatory regions are non-functional; therefore, complementary approaches, such as histone modification profiling or Hi-C, are needed to fully understand enhancer dynamics during liver regeneration. Finally, CRISPR-Cas9-mediated enhancer modifications could provide direct evidence of enhancer function in liver regeneration.

RESOURCE AVAILABILITY

Lead contact

Further information and requests for resources and reagents should be directed to and will be fulfilled by the lead contact, Montserrat Corominas (mcorominas@ub.edu).

Materials availability

This study did not generate new unique reagents.

Data and code availability

- The RNA-seq and ATAC-seq raw and processed data from this study are available at NCBI Gene Expression Omnibus under the accession numbers GEO: GSE181476 (RNA-seq)[33] and GEO: GSE266402 (ATAC-seq). This study did not generate any unique code.

- A Catalan version of the abstract, highlights, and graphical abstract is available at: https://doi.org/10.5281/zenodo.15267786

ACKNOWLEDGMENTS

We thank A.S. Nacht, T. Quesada-López, and E. Bertran for technical support; R. Corces for guidance on ATAC-seq; J. and P. Nieto for scRNA-seq advice; and the CRG Genomics Unit for assistance. We are also grateful to C. Camilleri-Robles for helpful discussions and manuscript revision. This project was funded by PID2021-123300NB-100 from MCIN/AEI/10.13039/501100011033/FEDER, UE to F.S and M.C.; 2021SGR00293 from the Agency for the Management of University and Research Grants (Generalitat de Catalunya) to M.C.; PID2021-122551OB-100 from MCIN/AEI/10.13039/501100011033/FEDER, UE to I.F.; and FPU20/01473 from the Spanish Ministerio de Universidades to P.L.G. We thank R. Guigó for financial support to M.R.R. and R.N. through grant PID2021-128956NB-I00 funded by MCIN/AEI/10.13039/501100011033/FEDER, UE. M.R.R. and R.N. acknowledge the support of the Spanish Ministry of Science and Innovation through the Centro de Excelencia Severo Ochoa (CEX2020-001049-S and MCIN/AEI/10.13039/501100011033) and the Generalitat de Catalunya through the CERCA program.

AUTHOR CONTRIBUTIONS

P.L.G., I.F., and M.C. conceived and designed the experiments. P.L.G. and M.H.I. performed the experiments. P.L.G., M.R.R., and R.N. analyzed the data. G.P.V. provided reagents and advice for the ATAC-seq experiments. P.L.G. and M.C. wrote the manuscript. P.L.G., M.R.R., G.P.V., F.S., I.F., R.N., and M.C. revised the manuscript. F.S., I.F., and M.C. acquired funding.

DECLARATION OF INTERESTS

The authors declare no competing interests.

DECLARATION OF GENERATIVE AI AND AI-ASSISTED TECHNOLOGIES

During the preparation of this work, the authors used ChatGPT to enhance the readability and language of the manuscript. After using this tool, the authors carefully reviewed and edited the content as needed and they take full responsibility for the content of the published article.

STAR★METHODS

Detailed methods are provided in the online version of this paper and include the following:

- KEY RESOURCES TABLE
- EXPERIMENTAL MODEL AND STUDY PARTICIPANT DETAILS
  - Animal procedures
- METHOD DETAILS
  - ATAC sequencing
  - Immunohistochemistry
  - Reporter assays
  - RNA sequencing data analysis
  - ATAC sequencing data analysis
  - ChIP sequencing data analysis
  - Hi-C data analysis
  - Enhancer-gene pair association
  - Single-cell RNA sequencing analysis
  - Transcription factor motif enrichment analysis
  - Gene coexpression regulatory network
  - Developmental analysis
- QUANTIFICATION AND STATISTICAL ANALYSIS

SUPPLEMENTAL INFORMATION

Supplemental information can be found online at https://doi.org/10.1016/j.xgen.2025.100887.

Received: July 7, 2024
Revised: March 10, 2025
Accepted: April 28, 2025
Published: May 22, 2025

REFERENCES

1. Goldman, J.A., and Poss, K.D. (2020). Gene regulatory programmes of tissue regeneration. Nat. Rev. Genet. *21*, 511–525. https://doi.org/10.1038/s41576-020-0239-7.
2. Rodriguez, A.M., and Kang, J. (2020). Regeneration enhancers: Starting a journey to unravel regulatory events in tissue regeneration. Semin. Cell Dev. Biol. *97*, 47–54. https://doi.org/10.1016/j.semcdb.2019.04.003.
3. Goldman, J.A., Kuzu, G., Lee, N., Karasik, J., Gemberling, M., Foglia, M. J., Karra, R., Dickson, A.L., Sun, F., Tolstorukov, M.Y., and Poss, K.D. (2017). Resolving Heart Regeneration by Replacement Histone Profiling. Dev. Cell *40*, 392–404.e5. https://doi.org/10.1016/j.devcel.2017.01.013.
4. Begeman, I.J., Shin, K., Osorio-Méndez, D., Kurth, A., Lee, N., Chamberlain, T.J., Pelegri, F.J., and Kang, J. (2020). Decoding an Organ Regeneration Switch by Dissecting Cardiac Regeneration Enhancers. Development *147*, dev.194019. https://doi.org/10.1242/dev.194019.
5. Kang, J., Hu, J., Karra, R., Dickson, A.L., Tornini, V.A., Nachtrab, G., Gemberling, M., Goldman, J.A., Black, B.L., and Poss, K.D. (2016). Modulation of tissue repair by regeneration enhancer elements. Nature *532*, 201–206. https://doi.org/10.1038/nature17644.
6. Wang, W., Hu, C.-K., Zeng, A., Alegre, D., Hu, D., Gotting, K., Ortega Granillo, A., Wang, Y., Robb, S., Schnittker, R., et al. (2020). Changes in regeneration-responsive enhancers shape regenerative capacities in vertebrates. Science *369*, eaaz3090. https://doi.org/10.1126/science.aaz3090.
7. Mokalled, M.H., Patra, C., Dickson, A.L., Endo, T., Stainier, D.Y.R., and Poss, K.D. (2016). Injury-induced *ctgfa* directs glial bridging and spinal cord regeneration in zebrafish. Science *354*, 630–634. https://doi.org/10.1126/science.aaf2679.
8. Harris, R.E., Setiawan, L., Saul, J., and Hariharan, I.K. (2016). Localized epigenetic silencing of a damage-activated WNT enhancer limits regeneration in mature Drosophila imaginal discs. Elife *5*, e11588. https://doi.org/10.7554/eLife.11588.
9. Vizcaya-Molina, E., Klein, C.C., Serras, F., Mishra, R.K., Guigó, R., and Corominas, M. (2018). Damage-responsive elements in *Drosophila* regeneration. Genome Res. *28*, 1852–1866. https://doi.org/10.1101/gr.233098.117.
10. Aguilar, C.A., Pop, R., Shcherbina, A., Watts, A., Matheny, R.W., Cacchiarelli, D., Han, W.M., Shin, E., Nakhai, S.A., Jang, Y.C., et al. (2016). Transcriptional and Chromatin Dynamics of Muscle Regeneration after Severe Trauma. Stem Cell Rep. *7*, 983–997. https://doi.org/10.1016/j.stemcr.2016.09.009.
11. Hung, H.A., Sun, G., Keles, S., and Svaren, J. (2015). Dynamic Regulation of Schwann Cell Enhancers after Peripheral Nerve Injury. J. Biol. Chem. *290*, 6937–6950. https://doi.org/10.1074/jbc.M114.622878.
12. Naik, S., Larsen, S.B., Gomez, N.C., Alaverdyan, K., Sendoel, A., Yuan, S., Polak, L., Kulukian, A., Chai, S., and Fuchs, E. (2017). Inflammatory memory sensitizes skin epithelial stem cells to tissue damage. Nature *550*, 475–480. https://doi.org/10.1038/nature24271.
13. Ge, Y., Gomez, N.C., Adam, R.C., Nikolova, M., Yang, H., Verma, A., Lu, C.P.-J., Polak, L., Yuan, S., Elemento, O., and Fuchs, E. (2017). Stem Cell Lineage Infidelity Drives Wound Repair and Cancer. Cell *169*, 636–650.e14. https://doi.org/10.1016/j.cell.2017.03.042.

14. Huang, G.N., Thatcher, J.E., McAnally, J., Kong, Y., Qi, X., Tan, W., DiMaio, J.M., Amatruda, J.F., Gerard, R.D., Hill, J.A., et al. (2012). C/EBP Transcription Factors Mediate Epicardial Activation During Heart Development and Injury. Science *338*, 1599–1603. https://doi.org/10.1126/science.1229765.

15. Vieira, J.M., Howard, S., Villa Del Campo, C., Bollini, S., Dubé, K.N., Masters, M., Barnette, D.N., Rohling, M., Sun, X., Hankins, L.E., et al. (2017). BRG1-SWI/SNF-dependent regulation of the Wt1 transcriptional landscape mediates epicardial activity during heart development and disease. Nat. Commun. *8*, 16034. https://doi.org/10.1038/ncomms16034.

16. Yan, R., Cigliola, V., Oonk, K.A., Petrover, Z., DeLuca, S., Wolfson, D.W., Vekstein, A., Mendiola, M.A., Devlin, G., Bishawi, M., et al. (2023). An enhancer-based gene-therapy strategy for spatiotemporal control of cargoes during tissue repair. Cell Stem Cell *30*, 96–111.e6. https://doi.org/10.1016/j.stem.2022.11.012.

17. Taub, R. (2004). Liver regeneration: from myth to mechanism. Nat. Rev. Mol. Cell Biol. *5*, 836–847. https://doi.org/10.1038/nrm1489.

18. Michalopoulos, G.K., and Bhushan, B. (2021). Liver regeneration: biological and pathological mechanisms and implications. Nat. Rev. Gastroenterol. Hepatol. *18*, 40–55. https://doi.org/10.1038/s41575-020-0342-4.

19. López-Luque, J., and Fabregat, I. (2018). Revisiting the liver: from development to regeneration - what we ought to know. Int. J. Dev. Biol. *62*, 441–451. https://doi.org/10.1387/ijdb.170264JL.

20. Blake, M.J., and Steer, C.J. (2023). Liver Regeneration in Acute on Chronic Liver Failure. Clin. Liver Dis. *27*, 595–616. https://doi.org/10.1016/j.cld.2023.03.005.

21. Arechederra, M., Berasain, C., Avila, M.A., and Fernández-Barrena, M.G. (2020). Chromatin dynamics during liver regeneration. Semin. Cell Dev. Biol. *97*, 38–46. https://doi.org/10.1016/j.semcdb.2019.03.004.

22. Zhang, C., Sun, C., Zhao, Y., Ye, B., and Yu, G. (2024). Signaling pathways of liver regeneration: Biological mechanisms and implications. iScience *27*, 108683. https://doi.org/10.1016/j.isci.2023.108683.

23. Bangru, S., and Kalsotra, A. (2020). Cellular and molecular basis of liver regeneration. Semin. Cell Dev. Biol. *100*, 74–87. https://doi.org/10.1016/j.semcdb.2019.12.004.

24. Aloia, L. (2021). Epigenetic Regulation of Cell-Fate Changes That Determine Adult Liver Regeneration After Injury. Front. Cell Dev. Biol. *9*, 643055. https://doi.org/10.3389/fcell.2021.643055.

25. Sato, Y., Katoh, Y., Matsumoto, M., Sato, M., Ebina, M., Itoh-Nakadai, A., Funayama, R., Nakayama, K., Unno, M., and Igarashi, K. (2017). Regulatory signatures of liver regeneration distilled by integrative analysis of mRNA, histone methylation, and proteomics. J. Biol. Chem. *292*, 8019–8037. https://doi.org/10.1074/jbc.M116.774547.

26. Wang, S., Zhang, C., Hasson, D., Desai, A., SenBanerjee, S., Magnani, E., Ukomadu, C., Lujambio, A., Bernstein, E., and Sadler, K.C. (2019). Epigenetic Compensation Promotes Liver Regeneration. Dev. Cell *50*, 43–56.e6. https://doi.org/10.1016/j.devcel.2019.05.034.

27. Zhang, C., Macchi, F., Magnani, E., and Sadler, K.C. (2021). Chromatin states shaped by an epigenetic code confer regenerative potential to the mouse liver. Nat. Commun. *12*, 4110. https://doi.org/10.1038/s41467-021-24466-1.

28. Wang, A.W., Wang, Y.J., Zahm, A.M., Morgan, A.R., Wangensteen, K.J., and Kaestner, K.H. (2020). The Dynamic Chromatin Architecture of the Regenerating Liver. Cell. Mol. Gastroenterol. Hepatol. *9*, 121–143. https://doi.org/10.1016/j.jcmgh.2019.09.006.

29. Merrell, A.J., Peng, T., Li, J., Sun, K., Li, B., Katsuda, T., Grompe, M., Tan, K., and Stanger, B.Z. (2021). Dynamic Transcriptional and Epigenetic Changes Drive Cellular Plasticity in the Liver. Hepatology *74*, 444–457. https://doi.org/10.1002/hep.31704.

30. Chen, T., Oh, S., Gregory, S., Shen, X., and Diehl, A.M. (2020). Single-cell omics analysis reveals functional diversification of hepatocytes during liver regeneration. JCI Insight *5*, e141024. https://doi.org/10.1172/jci.insight.141024.

31. Chembazhi, U.V., Bangru, S., Hernaez, M., and Kalsotra, A. (2021). Cellular plasticity balances the metabolic and proliferation dynamics of a regenerating liver. Genome Res. *31*, 576–591. https://doi.org/10.1101/gr.267013.120.

32. Xu, J., Guo, P., Hao, S., Shangguan, S., Shi, Q., Volpe, G., Huang, K., Zuo, J., An, J., Yuan, Y., et al. (2024). A spatiotemporal atlas of mouse liver homeostasis and regeneration. Nat. Genet. *56*, 953–969. https://doi.org/10.1038/s41588-024-01709-7.

33. Herranz-Itúrbide, M., López-Luque, J., Gonzalez-Sanchez, E., Caballero-Díaz, D., Crosas-Molist, E., Martín-Mur, B., Gut, M., Esteve-Codina, A., Jaquet, V., Jiang, J.X., et al. (2021). NADPH oxidase 4 (Nox4) deletion accelerates liver regeneration in mice. Redox Biol. *40*, 101841. https://doi.org/10.1016/j.redox.2020.101841.

34. Gralinska, E., Kohl, C., Sokhandan Fadakar, B., and Vingron, M. (2022). Visualizing Cluster-specific Genes from Single-cell Transcriptomics Data Using Association Plots. J. Mol. Biol. *434*, 167525. https://doi.org/10.1016/j.jmb.2022.167525.

35. Rib, L., Villeneuve, D., Minocha, S., Praz, V., Hernandez, N., Guex, N., and Herr, W.; CycliX Consortium (2018). Cycles of gene expression and genome response during mammalian tissue regeneration. Epigenetics Chromatin *11*, 52. https://doi.org/10.1186/s13072-018-0222-0.

36. Zhang, L., Huang, X., Meng, Z., Dong, B., Shiah, S., Moore, D.D., and Huang, W. (2009). Significance and Mechanism of CYP7a1 Gene Regulation during the Acute Phase of Liver Regeneration. Mol. Endocrinol. *23*, 137–145. https://doi.org/10.1210/me.2008-0198.

37. Zhao, Y., Ye, W., Wang, Y.-D., and Chen, W.-D. (2022). HGF/c-Met: A Key Promoter in Liver Regeneration. Front. Pharmacol. *13*, 808855. https://doi.org/10.3389/fphar.2022.808855.

38. Xu, C., Lin, F., and Qin, S. (2008). Relevance between lipid metabolism-associated genes and rat liver regeneration. Hepatol. Res. *38*, 825–837. https://doi.org/10.1111/j.1872-034X.2008.00345.x.

39. Chen, Y., Chen, L., Wu, X., Zhao, Y., Wang, Y., Jiang, D., Liu, X., Zhou, T., Li, S., Wei, Y., et al. (2023). Acute liver steatosis translationally controls the epigenetic regulator MIER1 to promote liver regeneration in a study with male mice. Nat. Commun. *14*, 1521. https://doi.org/10.1038/s41467-023-37247-9.

40. Sun, X., Chuang, J.-C., Kanchwala, M., Wu, L., Celen, C., Li, L., Liang, H., Zhang, S., Maples, T., Nguyen, L.H., et al. (2016). Suppression of the SWI/SNF Component Arid1a Promotes Mammalian Regeneration. Cell Stem Cell *18*, 456–466. https://doi.org/10.1016/j.stem.2016.03.001.

41. Shlyueva, D., Stampfel, G., and Stark, A. (2014). Transcriptional enhancers: from properties to genome-wide predictions. Nat. Rev. Genet. *15*, 272–286. https://doi.org/10.1038/nrg3682.

42. Pradeepa, M.M., Grimes, G.R., Kumar, Y., Olley, G., Taylor, G.C.A., Schneider, R., and Bickmore, W.A. (2016). Histone H3 globular domain acetylation identifies a new class of enhancers. Nat. Genet. *48*, 681–686. https://doi.org/10.1038/ng.3550.

43. Fulco, C.P., Nasser, J., Jones, T.R., Munson, G., Bergman, D.T., Subramanian, V., Grossman, S.R., Anyoha, R., Doughty, B.R., Patwardhan, T.A., et al. (2019). Activity-by-contact model of enhancer–promoter regulation from thousands of CRISPR perturbations. Nat. Genet. *51*, 1664–1669. https://doi.org/10.1038/s41588-019-0538-0.

44. Furlan-Magaril, M., Ando-Kuri, M., Arzate-Mejía, R.G., Morf, J., Cairns, J., Román-Figueroa, A., Tenorio-Hernández, L., Poot-Hernández, A.C., Andrews, S., Várnai, C., et al. (2021). The global and promoter-centric 3D genome organization temporally resolved during a circadian cycle. Genome Biol. *22*, 162. https://doi.org/10.1186/s13059-021-02374-3.

45. Falick Michaeli, T., Sabag, O., Azria, B., Fok, R., Abudi, N., Abramovitch, R., Monin, J., Gielchinsky, Y., Cedar, H., and Bergman, Y. (2024). Hepatocyte regeneration is driven by embryo-like DNA methylation reprogramming. Proc. Natl. Acad. Sci. USA *121*, e2314885121. https://doi.org/10.1073/pnas.2314885121.

46. López-Luque, J., Caballero-Díaz, D., Martinez-Palacián, A., Roncero, C., Moreno-Càceres, J., García-Bravo, M., Grueso, E., Fernández, A., Crosas-Molist, E., García-Álvaro, M., et al. (2016). Dissecting the role of epidermal growth factor receptor catalytic activity during liver regeneration and hepatocarcinogenesis. Hepatology *63*, 604–619. https://doi.org/10.1002/hep.28134.

47. Li, Z., Schulz, M.H., Look, T., Begemann, M., Zenke, M., and Costa, I.G. (2019). Identification of transcription factor binding sites using ATAC-seq. Genome Biol. *20*, 45. https://doi.org/10.1186/s13059-019-1642-2.

48. Argemí, J., Kress, T.R., Chang, H.C.Y., Ferrero, R., Bértolo, C., Moreno, H., González-Aparicio, M., Uriarte, I., Guembe, L., Segura, V., et al. (2017). X-box Binding Protein 1 Regulates Unfolded Protein, Acute-Phase, and DNA Damage Responses During Regeneration of Mouse Liver. Gastroenterology *152*, 1203–1216.e15. https://doi.org/10.1053/j.gastro.2016.12.040.

49. McLeay, R.C., and Bailey, T.L. (2010). Motif Enrichment Analysis: a unified framework and an evaluation on ChIP data. BMC Bioinf. *11*, 165. https://doi.org/10.1186/1471-2105-11-165.

50. Catarino, R.R., and Stark, A. (2018). Assessing sufficiency and necessity of enhancer activities for gene expression and the mechanisms of transcription activation. Genes Dev. *32*, 202–223. https://doi.org/10.1101/gad.310367.117.

51. Ertosun, M.G., Hapil, F.Z., and Osman Nidai, O. (2016). E2F1 transcription factor and its impact on growth factor and cytokine signaling. Cytokine Growth Factor Rev. *31*, 17–25. https://doi.org/10.1016/j.cytogfr.2016.02.001.

52. Li, W., Liang, X., Kellendonk, C., Poli, V., and Taub, R. (2002). STAT3 Contributes to the Mitogenic Response of Hepatocytes during Liver Regeneration. J. Biol. Chem. *277*, 28411–28417. https://doi.org/10.1074/jbc.M202807200.

53. Soubeyrand, S., Lau, P., and McPherson, R. (2023). Regulation of TRIB1 abundance in hepatocyte models in response to proteasome inhibition. Sci. Rep. *13*, 9320. https://doi.org/10.1038/s41598-023-36512-7.

54. Nault, R., Doskey, C.M., Fader, K.A., Rockwell, C.E., and Zacharewski, T. (2018). Comparison of Hepatic NRF2 and Aryl Hydrocarbon Receptor Binding in 2,3,7,8-Tetrachlorodibenzo- *p* -dioxin–Treated Mice Demonstrates NRF2-Independent PKM2 Induction. Mol. Pharmacol. *94*, 876–884. https://doi.org/10.1124/mol.118.112144.

55. Itoh, K., Chiba, T., Takahashi, S., Ishii, T., Igarashi, K., Katoh, Y., Oyake, T., Hayashi, N., Satoh, K., Hatayama, I., et al. (1997). An Nrf2/Small Maf Heterodimer Mediates the Induction of Phase II Detoxifying Enzyme Genes through Antioxidant Response Elements. Biochem. Biophys. Res. Commun. *236*, 313–322. https://doi.org/10.1006/bbrc.1997.6943.

56. Ishida, K., Kaji, K., Sato, S., Ogawa, H., Takagi, H., Takaya, H., Kawaratani, H., Moriya, K., Namisaki, T., Akahane, T., and Yoshiji, H. (2021). Sulforaphane ameliorates ethanol plus carbon tetrachloride-induced liver fibrosis in mice through the Nrf2-mediated antioxidant response and acetaldehyde metabolization with inhibition of the LPS/TLR4 signaling pathway. J. Nutr. Biochem. *89*, 108573. https://doi.org/10.1016/j.jnutbio.2020.108573.

57. Leonard, M.O., Kieran, N.E., Howell, K., Burne, M.J., Varadarajan, R., Dhakshinamoorthy, S., Porter, A.G., O'Farrelly, C., Rabb, H., and Taylor, C.T. (2006). Reoxygenation-specific activation of the antioxidant transcription factor Nrf2 mediates cytoprotective gene expression in ischemia-reperfusion injury. FASEB J. *20*, 2624–2626. https://doi.org/10.1096/fj.06-5097fje.

58. Gorkin, D.U., Barozzi, I., Zhao, Y., Zhang, Y., Huang, H., Lee, A.Y., Li, B., Chiou, J., Wildberg, A., Ding, B., et al. (2020). An atlas of dynamic chromatin landscapes in mouse fetal development. Nature *583*, 744–751. https://doi.org/10.1038/s41586-020-2093-3.

59. Kalhan, S., and Parimi, P. (2000). Gluconeogenesis in the fetus and neonate. Semin. Perinatol. *24*, 94–106. https://doi.org/10.1053/sp.2000.6360.

60. Perekatt, A.O., Valdez, M.J., Davila, M., Hoffman, A., Bonder, E.M., Gao, N., and Verzi, M.P. (2014). YY1 is indispensable for Lgr5+ intestinal stem cell renewal. Proc. Natl. Acad. Sci. USA *111*, 7695–7700. https://doi.org/10.1073/pnas.1400128111.

61. Pan, G., Diamanti, K., Cavalli, M., Lara Gutiérrez, A., Komorowski, J., and Wadelius, C. (2021). Multifaceted regulation of hepatic lipid metabolism by YY1. Life Sci. Alliance *4*, e202000928. https://doi.org/10.26508/lsa.202000928.

62. Zhang, S., Jiang, T., Feng, L., Sun, J., Lu, H., Wang, Q., Pan, M., Huang, D., Wang, X., Wang, L., and Jin, H. (2012). Yin Yang-1 suppresses differentiation of hepatocellular carcinoma cells through the downregulation of CCAAT/enhancer-binding protein alpha. J. Mol. Med. *90*, 1069–1077. https://doi.org/10.1007/s00109-012-0879-y.

63. Verheul, T.C.J., Van Hijfte, L., Perenthaler, E., and Barakat, T.S. (2020). The Why of YY1: Mechanisms of Transcriptional Regulation by Yin Yang 1. Front. Cell Dev. Biol. *8*, 592164. https://doi.org/10.3389/fcell.2020.592164.

64. Li, W., Yang, L., He, Q., Hu, C., Zhu, L., Ma, X., Ma, X., Bao, S., Li, L., Chen, Y., et al. (2019). A Homeostatic Arid1a-Dependent Permissive Chromatin State Licenses Hepatocyte Responsiveness to Liver-Injury-Associated YAP Signaling. Cell Stem Cell *25*, 54–68.e5. https://doi.org/10.1016/j.stem.2019.06.008.

65. Walesky, C.M., Kolb, K.E., Winston, C.L., Henderson, J., Kruft, B., Fleming, I., Ko, S., Monga, S.P., Mueller, F., Apte, U., et al. (2020). Functional compensation precedes recovery of tissue mass following acute liver injury. Nat. Commun. *11*, 5785. https://doi.org/10.1038/s41467-020-19558-3.

66. Chen, F., Schönberger, K., and Tchorz, J.S. (2023). Distinct hepatocyte identities in liver homeostasis and regeneration. JHEP Rep. *5*, 100779. https://doi.org/10.1016/j.jhepr.2023.100779.

67. Ma, X., Huang, T., Chen, X., Li, Q., Liao, M., Fu, L., Huang, J., Yuan, K., Wang, Z., and Zeng, Y. (2025). Molecular mechanisms in liver repair and regeneration: from physiology to therapeutics. Signal Transduct. Target. Ther. *10*, 63. https://doi.org/10.1038/s41392-024-02104-8.

68. Solhi, R., Lotfinia, M., Gramignoli, R., Najimi, M., and Vosough, M. (2021). Metabolic hallmarks of liver regeneration. Trends Endocrinol. Metab. *32*, 731–745. https://doi.org/10.1016/j.tem.2021.06.002.

69. Uriarte, I., Santamaria, E., López-Pascual, A., Monte, M.J., Argemí, J., Latasa, M.U., Adán-Villaescusa, E., Irigaray, A., Herranz, J.M., Arechederra, M., et al. (2024). New insights into the regulation of bile acids synthesis during the early stages of liver regeneration: A human and experimental study. Biochim. Biophys. Acta BBA - Mol. Basis Dis. *1870*, 167166. https://doi.org/10.1016/j.bbadis.2024.167166.

70. Slabber, C.F., Bachofner, M., Speicher, T., Kuklin, A., Fearon, A.E., Padrissa-Altés, S., Bogorad, R., Horváth Rudigier, C., Wüst, D., Krautbauer, S., et al. (2023). The ubiquitin ligase Uhrf2 is a master regulator of cholesterol biosynthesis and is essential for liver regeneration. Sci. Signal. *16*, eade8029. https://doi.org/10.1126/scisignal.ade8029.

71. Živný, P., Živná, H., Palička, V., Žaloudková, L., Mocková, P., Cermanová, J., and Mičuda, S. (2018). Modulation of Rat Liver Regeneration after Partial Hepatectomy by Dietary Cholesterol. Acta Medica Hradec Kralove Czech Repub *61*, 22–28. https://doi.org/10.14712/18059694.2018.19.

72. Behrens, A., Sibilia, M., David, J.P., Möhle-Steinlein, U., Tronche, F., Schütz, G., and Wagner, E.F. (2002). Impaired postnatal hepatocyte proliferation and liver regeneration in mice lacking c-jun in the liver. EMBO J. *21*, 1782–1790. https://doi.org/10.1093/emboj/21.7.1782.

73. Jia, X., Lin, W., and Wang, W. (2023). Regulation of chromatin organization during animal regeneration. Cell Regen. *12*, 19. https://doi.org/10.1186/s13619-023-00162-x.

74. Cao, Y., Xia, Y., Balowski, J.J., Ou, J., Song, L., Safi, A., Curtis, T., Crawford, G.E., Poss, K.D., and Cao, J. (2022). Identification of enhancer regulatory elements that direct epicardial gene expression during zebrafish

heart regeneration. Development *149*, dev200133. https://doi.org/10.1242/dev.200133.

75. Hishida, T., Yamamoto, M., Hishida-Nozaki, Y., Shao, C., Huang, L., Wang, C., Shojima, K., Xue, Y., Hang, Y., Shokhirev, M., et al. (2022). In vivo partial cellular reprogramming enhances liver plasticity and regeneration. Cell Rep. *39*, 110730. https://doi.org/10.1016/j.celrep.2022.110730.

76. Hsu, J.C., Laz, T., Mohn, K.L., and Taub, R. (1991). Identification of LRF-1, a leucine-zipper protein that is rapidly and highly induced in regenerating liver. Proc. Natl. Acad. Sci. USA *88*, 3511–3515. https://doi.org/10.1073/pnas.88.9.3511.

77. Allan, A.L., Albanese, C., Pestell, R.G., and LaMarre, J. (2001). Activating Transcription Factor 3 Induces DNA Synthesis and Expression of Cyclin D1 in Hepatocytes. J. Biol. Chem. *276*, 27272–27280. https://doi.org/10.1074/jbc.M103196200.

78. Cui, A., Ding, D., and Li, Y. (2021). Regulation of Hepatic Metabolism and Cell Growth by the ATF/CREB Family of Transcription Factors. Diabetes *70*, 653–664. https://doi.org/10.2337/dbi20-0006.

79. Milland, J., and Schreiber, G. (1991). Transcriptional activity of the phosphoenolpyruvate carboxykinase gene decreases in regenerating rat liver. FEBS Lett. *279*, 184–186. https://doi.org/10.1016/0014-5793(91)80144-R.

80. Xu, Y., Li, Y., Jadhav, K., Pan, X., Zhu, Y., Hu, S., Chen, S., Chen, L., Tang, Y., Wang, H.H., et al. (2021). Hepatocyte ATF3 protects against atherosclerosis by regulating HDL and bile acid metabolism. Nat. Metab. *3*, 59–74. https://doi.org/10.1038/s42255-020-00331-1.

81. Beyer, T.A., Xu, W., Teupser, D., Auf Dem Keller, U., Bugnon, P., Hildt, E., Thiery, J., Kan, Y.W., and Werner, S. (2008). Impaired liver regeneration in Nrf2 knockout mice: role of ROS-mediated insulin/IGF-1 resistance. EMBO J. *27*, 212–223. https://doi.org/10.1038/sj.emboj.7601950.

82. Chan, B.K.Y., Elmasry, M., Forootan, S.S., Russomanno, G., Bunday, T. M., Zhang, F., Brillant, N., Starkey Lewis, P.J., Aird, R., Ricci, E., et al. (2021). Pharmacological Activation of Nrf2 Enhances Functional Liver Regeneration. Hepatology *74*, 973–986. https://doi.org/10.1002/hep.31859.

83. Wang, X., Kiyokawa, H., Dennewitz, M.B., and Costa, R.H. (2002). The Forkhead Box m1b transcription factor is essential for hepatocyte DNA replication and mitosis during mouse liver regeneration. Proc. Natl. Acad. Sci. USA *99*, 16881–16886. https://doi.org/10.1073/pnas.252570299.

84. Suzuki, N., and Ochi, H. (2020). Regeneration enhancers: A clue to reactivation of developmental genes. Dev. Growth Differ. *62*, 343–354. https://doi.org/10.1111/dgd.12654.

85. Harris, R.E. (2022). Regeneration enhancers: a field in development. Am. J. Physiol. Cell Physiol. *323*, C1548–C1554. https://doi.org/10.1152/ajpcell.00403.2022.

86. Li, L., Cui, L., Lin, P., Liu, Z., Bao, S., Ma, X., Nan, H., Zhu, W., Cen, J., Mao, Y., et al. (2023). Kupffer-cell-derived IL-6 is repurposed for hepatocyte dedifferentiation via activating progenitor genes from injury-specific enhancers. Cell Stem Cell *30*, 283–299.e9. https://doi.org/10.1016/j.stem.2023.01.009.

87. Dobin, A., Davis, C.A., Schlesinger, F., Drenkow, J., Zaleski, C., Jha, S., Batut, P., Chaisson, M., and Gingeras, T.R. (2013). STAR: ultrafast universal RNA-seq aligner. Bioinformatics *29*, 15–21. https://doi.org/10.1093/bioinformatics/bts635.

88. Li, B., and Dewey, C.N. (2011). RSEM: accurate transcript quantification from RNA-Seq data with or without a reference genome. BMC Bioinf. *12*, 323. https://doi.org/10.1186/1471-2105-12-323.

89. Yu, G., Wang, L.-G., Han, Y., and He, Q.-Y. (2012). clusterProfiler: an R Package for Comparing Biological Themes Among Gene Clusters. OMICS A J. Integr. Biol. *16*, 284–287. https://doi.org/10.1089/omi.2011.0118.

90. Love, M.I., Huber, W., and Anders, S. (2014). Moderated estimation of fold change and dispersion for RNA-seq data with DESeq2. Genome Biol. *15*, 550. https://doi.org/10.1186/s13059-014-0550-8.

91. Bolger, A.M., Lohse, M., and Usadel, B. (2014). Trimmomatic: a flexible trimmer for Illumina sequence data. Bioinformatics *30*, 2114–2120. https://doi.org/10.1093/bioinformatics/btu170.

92. Langmead, B., and Salzberg, S.L. (2012). Fast gapped-read alignment with Bowtie 2. Nat. Methods *9*, 357–359. https://doi.org/10.1038/nmeth.1923.

93. Tarasov, A., Vilella, A.J., Cuppen, E., Nijman, I.J., and Prins, P. (2015). Sambamba: fast processing of NGS alignment formats. Bioinforma. Oxf. Engl. *31*, 2032–2034. https://doi.org/10.1093/bioinformatics/btv098.

94. Zhang, Y., Liu, T., Meyer, C.A., Eeckhoute, J., Johnson, D.S., Bernstein, B.E., Nusbaum, C., Myers, R.M., Brown, M., Li, W., and Liu, X.S. (2008). Model-based analysis of ChIP-Seq (MACS). Genome Biol. *9*, R137. https://doi.org/10.1186/gb-2008-9-9-r137.

95. Pohl, A., and Beato, M. (2014). bwtool: a tool for bigWig files. Bioinforma. Oxf. Engl. *30*, 1618–1619. https://doi.org/10.1093/bioinformatics/btu056.

96. Li, H., and Durbin, R. (2009). Fast and accurate short read alignment with Burrows–Wheeler transform. Bioinformatics *25*, 1754–1760. https://doi.org/10.1093/bioinformatics/btp324.

97. Durand, N.C., Shamim, M.S., Machol, I., Rao, S.S.P., Huntley, M.H., Lander, E.S., and Aiden, E.L. (2016). Juicer Provides a One-Click System for Analyzing Loop-Resolution Hi-C Experiments. Cell Syst. *3*, 95–98. https://doi.org/10.1016/j.cels.2016.07.002.

98. Hao, Y., Stuart, T., Kowalski, M.H., Choudhary, S., Hoffman, P., Hartman, A., Srivastava, A., Molla, G., Madad, S., Fernandez-Granda, C., and Satija, R. (2024). Dictionary learning for integrative, multimodal and scalable single-cell analysis. Nat. Biotechnol. *42*, 293–304. https://doi.org/10.1038/s41587-023-01767-y.

99. Korsunsky, I., Millard, N., Fan, J., Slowikowski, K., Zhang, F., Wei, K., Baglaenko, Y., Brenner, M., Loh, P.R., and Raychaudhuri, S. (2019). Fast, sensitive and accurate integration of single-cell data with Harmony. Nat. Methods *16*, 1289–1296. https://doi.org/10.1038/s41592-019-0619-0.

100. Danecek, P., Bonfield, J.K., Liddle, J., Marshall, J., Ohan, V., Pollard, M. O., Whitwham, A., Keane, T., McCarthy, S.A., Davies, R.M., and Li, H. (2021). Twelve years of SAMtools and BCFtools. GigaScience *10*, giab008. https://doi.org/10.1093/gigascience/giab008.

101. Shannon, P., Markiel, A., Ozier, O., Baliga, N.S., Wang, J.T., Ramage, D., Amin, N., Schwikowski, B., and Ideker, T. (2003). Cytoscape: A Software Environment for Integrated Models of Biomolecular Interaction Networks. Genome Res. *13*, 2498–2504. https://doi.org/10.1101/gr.1239303.

102. Higgins, M., and Anderson, R.M. (1931). Experimental pathology of liver: restoration of liver of white rat following partial surgical removal. Arch. Pathol. Lab Med. *12*, 186–202.

103. Corces, M.R., Trevino, A.E., Hamilton, E.G., Greenside, P.G., Sinnott-Armstrong, N.A., Vesuna, S., Satpathy, A.T., Rubin, A.J., Montine, K.S., Wu, B., et al. (2017). An improved ATAC-seq protocol reduces background and enables interrogation of frozen tissues. Nat. Methods *14*, 959–962. https://doi.org/10.1038/nmeth.4396.

104. Buenrostro, J.D., Wu, B., Chang, H.Y., and Greenleaf, W.J. (2015). ATAC-seq: A Method for Assaying Chromatin Accessibility Genome-Wide. Curr. Protoc. Mol. Biol. *109*, 21.29.1–21.29.9. https://doi.org/10.1002/0471142727.mb2129s109.

105. Fazio, E.N., Young, C.C., Toma, J., Levy, M., Berger, K.R., Johnson, C.L., Mehmood, R., Swan, P., Chu, A., Cregan, S.P., et al. (2017). Activating transcription factor 3 promotes loss of the acinar cell phenotype in response to cerulein-induced pancreatitis in mice. Mol. Biol. Cell *28*, 2347–2359. https://doi.org/10.1091/mbc.e17-04-0254.

106. Nguyen, H.C.B., Adlanmerini, M., Hauck, A.K., and Lazar, M.A. (2020). Dichotomous engagement of HDAC3 activity governs inflammatory responses. Nature *584*, 286–290. https://doi.org/10.1038/s41586-020-2576-2.

107. Seidman, J.S., Troutman, T.D., Sakai, M., Gola, A., Spann, N.J., Bennett, H., Bruni, C.M., Ouyang, Z., Li, R.Z., Sun, X., et al. (2020). Niche-Specific Reprogramming of Epigenetic Landscapes Drives Myeloid Cell Diversity in Nonalcoholic Steatohepatitis. Immunity *52*, 1057–1074.e7. https://doi.org/10.1016/j.immuni.2020.04.001.

108. Huang, M., Wang, X., Zhang, M., Liu, Y., and Chen, Y.-G. (2024). METTL3 restricts RIPK1-dependent cell death via the ATF3-cFLIP axis in the intestinal epithelium. Cell Regen. *13*, 14. https://doi.org/10.1186/s13619-024-00197-8.

STAR★METHODS

KEY RESOURCES TABLE

REAGENT or RESOURCE	SOURCE	IDENTIFIER
Antibodies		
Anti-ATF3 antibody [EPR19488]	Abcam	ab207434; RRID: AB_2734728
Critical commercial assays		
Nano-GLO® Dual-Luciferase Reporter Assay Kit	Promega	N1610
Optiprep Density Gradient Medium	Sigma-Aldrich	D1556
Deposited data		
RNA-seq liver regeneration post-PHx (6h, 24h, 48h)	https://doi.org/10.1016/j.redox.2020.101841	GEO: GSE181476
ATAC-seq liver regeneration post-PHx (6h, 24h, 48h)	Present study	GEO: GSE266402
ChIP-seq H3K27ac in liver pre-PHx (0 h)	https://doi.org/10.1038/s41467-023-37247-9	GEO: GSE188742
ChIP-seq H3K27ac in liver, post-PHx (40 h)	https://doi.org/10.1016/j.stem.2016.03.001	GEO: GSE76935
ChIP-seq Atf3 in Intestinal organoids	https://doi.org/10.1186/s13619-024-00197-8	GEO: GSE262282
ChIP-seq Atf3 in bone marrow macrophages	https://doi.org/10.1038/s41586-020-2576-2	GEO: GSE140581
ChIP-seq Atf3 in hepatic macrophages	https://doi.org/10.1016/j.immuni.2020.04.001	GEO: GSE128336
ChIP-seq Atf3 in pancreatic tissue	https://doi.org/10.1091/mbc.e17-04-0254	GEO: GSE60250
ChIP-seq Nrf2 in liver	https://doi.org/10.1124/mol.118.112144	GEO: GSE109865
Hi-C liver	https://doi.org/10.1186/s13059-021-02374-3	GEO: GSE155158
scRNA-seq liver regeneration post-PHx (0h, 24h, 48h)	https://doi.org/10.1101/gr.267013.120	GEO: GSE151309
ATAC-seq liver development	https://doi.org/10.1038/s41586-020-2093-3	GEO: GSE172627
Experimental models: Cell lines		
Immortalised hepatocytes	López-Luque et al.[46]	https://doi.org/10.1002/hep.28134
Experimental models: Organisms/strains		
Mouse: C57BL/6J	The Jackson Laboratory	RRID: IMSR_JAX:000664
Oligonucleotides		
Primer: ATACseqPeak_39376 cloning primer forward: GTAGCTAGCGGAATGGGATGGGGAGACAG	This paper	N/A
Primer: ATACseqPeak_39376 cloning primer reverse: ATGAAGCTTCTCAGCCCAAATTCAGATGG	This paper	N/A
Primer: ATACseqPeak_76443 cloning primer forward: GTAGCTAGCGCTTGCCTGAACCCTTCTCC	This paper	N/A
Primer: ATACseqPeak_76443 cloning primer reverse: ATGAAGCTTCCTAAGCCCGTAACAGGACC	This paper	N/A
Primer: ATACseqPeak_69905 cloning primer forward: GTAGCTAGCCAGCTTTGGACTGTCTGCTC	This paper	N/A
Primer: ATACseqPeak_69905 cloning primer reverse: ATGAAGCTTGTGTGTACCAGTTCGAAGTG	This paper	N/A
Primer: ATACseqPeak_9588 cloning primer forward: GTAGCTAGCCAGGACGAGTACTTCACCAG	This paper	N/A

(*Continued on next page*)

Continued

REAGENT or RESOURCE	SOURCE	IDENTIFIER
Primer: ATACseqPeak_9588 cloning primer reverse: ATGAAGCTTCCATGAAGAAGGGCAAGTGC	This paper	N/A
Primer: ATACseqPeak_70885 cloning primer forward: CTGCGGGCTAGCAGTAGAAG	This paper	N/A
Primer: ATACseqPeak_70885 cloning primer reverse: ATGAAGCTTGACCTGACTCCTGGTCTGTC	This paper	N/A
Primer: ATACseqPeak_57343 cloning primer forward: GTAGCTAGCTCCTCTGTGTTGAAGAAGGC	This paper	N/A
Primer: ATACseqPeak_57343 cloning primer reverse: ATGAAGCTTCCAGGCTAGGATGTGATAGC	This paper	N/A
Recombinant DNA		
Plasmid: pGL4.27[luc2P/minP/Hygro]	Promega	E8451
Plasmid: pNL1.1.TK[Nluc/TK] Vector	Promega	N1501
Plasmid: Atf3 (NM_007498) Mouse Tagged ORF Clone	Origene	MR201634
Plasmid: Nfe2l2 (NM_010902) Mouse Tagged ORF Clone	Origene	MR226717
Software and algorithms		
grape-nf	in-house	https://github.com/guigolab/grape-nf
STAR 2.4.0	Dobin et al.[87]	
RSEM	Li et al.[88]	
clusterProfiler	Yu et al.[89]	
heatmap3		https://github.com/slzhao/heatmap3
DESeq2	Love et al.[90]	N/A
Trimmomatic	Bolger et al.[91]	N/A
Bowtie2	Langmead et al.[92]	N/A
Sambamba	Tarasov et al.[93]	N/A
MACS2	Zhang et al.[94]	N/A
bwtool	Pohl et al.[95]	N/A
BWA	Li et al.[96]	N/A
Juicer	Durand et al.[97]	N/A
Activity-by-contact algorithm	Fulco et al.[43]	N/A
Seurat v5.0.3	Hao et al.[98]	N/A
Harmony v1.2.0	Korsunsky et al.[99]	N/A
HINT-ATAC	Li et al.[47]	N/A
SAMtools v.1.16	Danecek et al.[100]	N/A
MEME Suite 5.4.1	McLeay et al.[49]	N/A
Cytoscape Software v3.10.2	Shannon et al.[101]	N/A

EXPERIMENTAL MODEL AND STUDY PARTICIPANT DETAILS

Animal procedures

C57BL/6J wild-type (WT) mice were obtained from Jackson Laboratories and housed at the IDIBELL (Barcelona, Spain). All experiments complied with the EU Directive 2010/63/UE for animal experiments and the institution's guidelines (Ethics Committee for Animal Experimentation of the IDIBELL) and were approved by the General Direction of Environment and Biodiversity, Government of

Catalonia (experiments #4589). Animals were 8 to 16-week-old male and female mice, housed under a 12h light/dark cycle with free access to food and water. Partial hepatectomies (PHx) were performed by removing two-thirds of the adult mouse liver, as described by Higgins and Anderson (1931).[102] The mice that had undergone surgery without liver resection (sham-operated) were used as controls. The mice were euthanised 6, 24 and 48 h after surgery, and their liver lobes were immediately frozen in liquid nitrogen and stored at −80°C. The same livers used to extract RNA were used to prepare the ATAC-seq libraries. The number of animals used in the study was minimised for ethical reasons. Thus, 2 hepatectomised and 1–2 sham-operated animals were used for each time point after surgery.

METHOD DETAILS

ATAC sequencing

ATAC-seq libraries were prepared following the Omni-ATAC protocol[103] with minor modifications. Briefly, 10–20 mg of frozen liver were placed in a pre-chilled Tenbroeck tissue grinder containing 1 mL of the Omni-ATAC homogenisation buffer and let thaw for 5 min. The tissue was homogenised on ice using a glass Tenbroeck grinder and then filtered through a 70μm Flowmi strainer. Nuclei were pelleted for 5 min at 350 g and isolated using iodixanol density gradient centrifugation (OptiPrep). The nucleus band was transferred to a fresh tube and diluted in ATAC-seq resuspension buffer (ATAC-RSB)-Tween. Nuclei were counted using trypan blue staining and 50,000 nuclei were aliquoted per sample and resuspended in 50 μL of the transposition mixture (25 μL of 2× TD buffer (Illumina, San Francisco, CA), 2.5 μL of transposase (Illumina, San Francisco, CA), 16.5 μL of PBS, 0.5 μL of 1% digitonin, 0.5 μL of 10% Tween 20 and 5 μL of H_2O). Transposition reactions were incubated at 37°C for 30 min in a thermomixer at 1,000 RPM. Reactions were cleaned up with the Qiagen MinElute PCR Purification Kit (Qiagen, Frederick, MD) and eluted into 10 μL of the elution buffer. Purified DNA was used to prepare the ATAC-seq libraries, as described previously.[104] The quality of the tagmented libraries was visualised with the Agilent Bioanalyzer High Sensitivity DNA Assay (Agilent Technologies, Savage, DE) and sequenced on the HiSeq2500 platform at the Center for Genomic Regulation (CRG) sequencing facility in Barcelona, Spain. A minimum of 49 million paired-end 50-bp-long reads were obtained per sample.

Immunohistochemistry

Paraffin-embedded tissues were cut into 4-μm-thick sections. Immunohistochemical (IHC) analyses were performed using standard procedures.[33] Sections were incubated overnight at 4°C with a recombinant anti-ATF3 antibody (1:100; ab207434, Abcam). Binding was developed with the VECTASTAIN ABC HRP Kit (rabbit IgG; PK-4001, Vector Laboratories). Tissues were visualised and imaged under a microscope.

Reporter assays

Candidate RREs were amplified from mouse genomic DNA using the primers listed in key resources table and cloned into the pGL4.27[luc2P/minP/Hygro] plasmid (Promega). NheI and HindIII restriction sites were added to the 5′ ends of the forward and reverse primers, respectively, to facilitate directional cloning. The amplified PCR products of RREs and the pGL4.27 plasmid were double digested with NheI-HF and HindIII-HF restriction enzymes (New England Biolabs), followed by dephosphorylation of the 5′ ends of the digested plasmid using calf intestinal alkaline phosphatase (0.01u CIAP/pmol of DNA ends). After digestion, the PCR-amplified inserts and the linearized vector were purified and then ligated at a 1:3 vector-to-insert ratio using T4 DNA ligase (New England Biolabs), following the manufacturer's instructions. The ligation products were transformed into DH5α competent cells (Invitrogen), and successfully transformed Ampicillin-resistant colonies were confirmed by sequencing.

In-house immortalised hepatocyte cell line[46] was grown in Dulbecco's Modified Eagle Medium (DMEM) supplemented with 10% fetal bovine serum (FBS) (Sera Laboratories International Ltd, West Sussex, UK), Penicillin (100 U/mL), Streptomycin (100 μg/mL), Amphotericin (2.5 μg/mL) and L-glutamine (2 mM), and maintained in a humidified atmosphere of 37°C, 5% CO2. Cells seeded in 12-well plates at a density of 3 x 10^4 cells per well were transiently cotransfected using polyethylenimine (3μL PEI/μg DNA) with 995 ng/mL of DNA reporter of interest per well (recombinant pGL4.24 [luc2P/minP/Hygro]) and 5 ng/mL of NanoLuc plasmid (N1501, Promega, Madison, WI, USA) in complete media. 16 h post-transfection, the medium was replaced, and cells were serum-starved for 24 h. After, cells were either switched to complete medium with 10% FBS or continued serum starvation for an additional 3 h. Cells were then harvested, lysed, and luciferase activities were measured using the Nano-GLO Dual-Luciferase Reporter Assay Kit (Promega, Madison, WI, USA) following the manufacturer's instructions. Firefly luciferase signal was divided by the NanoLuc signal to determine relative luciferase activity. The activity for each luciferase construct was normalised for the activity of the minimal promoter (minP). The constructs were measured in two independent experiments in a total of six biological replicates. Statistical significance was assessed using two-way ANOVA followed by Tukey's Honest Significant Difference (Tukey's HSD) test to compare each construct against minP, and to compare between starvation and FBS-treatment. Normality and homogeneity of variance were assumed. All tests were two-sided. Differences were considered statistically significant when p-value was <0.05.

Validation of transcriptional activators was performed following the same experimental conditions with minor modifications. Cells were transiently cotransfected with 800 ng/mL of luciferase reporter, 195 ng of mouse ATF3 plasmid (MR201634, Origene) or mouse Nfe2l2 plasmid (MR226717, Origene), and 5 ng/mL of NanoLuc plasmid (N1501, Promega, Madison, WI, USA) in complete media. 16 h post-transfection, the medium was replaced and 24 h later cells were harvested, lysed, and luciferase activities were measured

using the Nano-GLO Dual-Luciferase Reporter Assay Kit (Promega, Madison, WI, USA) following the manufacturer's instructions. The constructs were measured in two independent experiments in a total of six biological replicates. Statistical significance was assessed using one-way ANOVA followed by Tukey's HSD. Normality and homogeneity of variance were assumed. All tests were two-sided. Differences were considered statistically significant when p-value was <0.05.

RNA sequencing data analysis

RNA-seq raw data for WT mice at 6, 24 and 48 h after PHx were downloaded from GEO accession number GSE181476[33] and processed using the in-house pipeline grape-nf (available at https://github.com/guigolab/grape-nf). RNA-seq reads were aligned to the *Mus musculus* genome assembly GRCm39 using the STAR 2.4.0 software[87] allowing up to 4 mismatches per paired alignment. We used the mouse genome GENCODE annotation vM27. Only alignments for reads mapping to ten or fewer loci were reported. Genes and transcripts per kilobase million (TPMs) were quantified using RSEM.[88] Tracks were visualised with the UCSC Genome Browser. From the RNA-seq data, the expression values for 55,360 annotated genes were estimated and the gene expression matrix was quantile normalised. Only genes with >1 TPM in at least one condition were considered for subsequent analyses (11,512 genes). Correspondence analysis and association plots[34] were used to cluster and identify the genes with differential expression profiles during early liver regeneration. Briefly, we used the APL R package, considering 5 dimensions and clusters were defined setting a threshold of Sα score > -0.05. Normalised expression values as z-scores were used to visualise differential expressed genes using line plots or hierarchical clustering from heatmap3 R package. Gene Ontology enrichment analysis of the clusters of interest was performed using the Bioconductor package clusterProfiler,[89] one-sided Fisher's exact test was applied and p-adjust <0.05 was used as cut-off, no assumptions about the underlying distribution of gene expression data was done. Differential gene expression analysis of the TFs from Figure 4 was performed using DESeq2[90] using Wald test, assuming negative binomial distribution.

ATAC sequencing data analysis

Reads were trimmed *in silico* to remove adapter sequences and low-quality reads using Trimmomatic[91] while FastQC was used to check their quality. The reads were aligned to the mouse (mm39) reference genome using Bowtie2.[92] Duplicate reads were removed using Picard (http://broadinstitute.github.io/picard/), and the mitochondrial reads and the reads mapping to the ENCODE blacklisted regions were filtered out using BEDTools2. Sambamba[93] was used to eliminate fragments larger than 400 bp. Peak calling was performed using a MACS2[94] run in the pair-end mode, requesting an p-adjust <0.01. Read depth-normalised values (pileup) were generated by MACS2 and stored in bigWig files. All the ATAC-seq samples were checked for the library complexity and PCR bottlenecking following ENCODE standards https://www.encodeproject.org/data-standards/terms/#library (Table S6). Each replicate, time point and condition in the ATAC-seq data was processed independently. However, we combined the data, processing together the read alignments from all 6 experiments in the regenerated livers. The peaks that had at least 50% overlap in each replicate in at least one condition were retained, while the peaks with an overlap smaller than 25 nucleotides were discarded. The maximum heights of all the peaks were then quantified for each sample using bwtool.[95] These values were quantile-normalised among the samples and the peak heights were averaged between replicates (Table S7). Differentially accessible regions were identified using an absolute fold-change larger than 1.7 as the cut-off between regeneration and control at each time point. These regions were classified into *de novo* (open regions detected exclusively in REG), increasing (both in CTRL and REG, and at least 1.7-fold higher in REG) or decreasing peaks (1.7-fold lower in REG). Finally, the peaks were classified into promoters (+-500 bp around the TSS), proximal enhancers (+-500 bp away from promoters) or distal enhancers (>1 kb from the TSS), considering all possible protein-coding and non-coding isoforms from the GENCODE mouse annotation vM27.

ChIP sequencing data analysis

ChIP-seq raw read data corresponding to H3K27ac histone modification pre-PHx[39] and post-PHx[40] as well as NRF2 binding in intact liver[54] and ATF3 binding in different tissues[105–108] were obtained from NCBI GEO. Reads were aligned to the *Mus musculus* genome assembly GRCm39 with BWA.[96] Peak calling was performed using MACS2,[94] applying a cut-off of 0.05 for the FDR. Fold changes in relation to input control data were calculated and converted into the BigWig format. All the ChIP-seq samples were checked for the library complexity and PCR bottlenecking following ENCODE standards https://www.encodeproject.org/data-standards/terms/#library (Table S6). The presence of H3K27ac around RREs was analyzed by extending the ATAC-seq peaks to 500 bp to incorporate the flanking nucleosomes and using BEDTools2 intersectBed with default conditions. The overlap between ATAC-seq peaks and NRF2 and ATF3 ChIP-seq peaks was analyzed using BEDTools intersectBed with default conditions. The statistical significance of this overlap between the ATF3 peaks and the *de novo* and increasing peaks, and between the NRF2 peaks and the increasing peaks was calculated using BEDTools2 Fisher's exact test.

Hi-C data analysis

Raw read sequences for *in situ* and promoter-capture Hi-C from intact livers[44] were downloaded from NCBI GEO under the accession number GSE155161. The Juicer pipeline[97] was used to process these data. In brief, paired-end reads were mapped to the *Mus musculus* genome assembly GRCm39 with BWA,[96] keeping the most 5′ alignment block. The custom-made Juicer script ''chimeric_blacklist.awk'' was used to select the proper pair alignments. These alignments in turn were sorted and duplicates were removed. Hi-C matrices were generated with the Juicer Pre command, using standard resolutions of up to 5 kb and the SCALE normalisation

method. To calculate the contact probability of the promoter and enhancer regions, these regions were projected onto particular 5-kb genomic intervals and before calculating the probability as a fraction of the normalised read counts supporting the interaction of the promoter and enhancer intervals (n-th diagonal) divided by the normalised read counts supporting the interaction of the promoter with itself (zero-diagonal). The generated Hi-C contact matrices were also used to calculate the background contact probabilities by averaging contact probabilities genome-wide across contacting regions at the same distance and using these average values to impute contact probabilities to the regions that are absent in the Hi-C matrices due to their low mappability.

Enhancer-gene pair association

Proximal peaks were classified as proximal enhancers and associated with the nearby promoters directly. For distal peaks, the activity-by-contact (ABC) algorithm[43] was implemented. The activity of the corresponding regions was calculated as a geometric mean of the ATAC-seq and H3K27ac signals. The maximum pileup signal across all the regeneration samples combined (see above) was used as a source of the ATAC-seq data. The maximum fold-change from the regenerated livers (GEO: GSE76935)[40] was used as a source of H3K27ac data. H3K27ac was determined in nucleosomes adjusted to the open chromatin regions, extending these regions by 250 bp in both directions. All enhancers lying closer than 2 Mb up- or downstream of the corresponding promoter were considered candidate regulatory elements. The maximum value from the *in situ* Hi-C, promoter-capture Hi-C or the same distance background control was used to calculate the contact probabilities of the promoter and enhancer regions. The activity of the promoter was included in the prediction model, assuming the contact probability of the promoter with itself to be equal to one. ABC scores were calculated for the promoter and each candidate enhancer by multiplying the activity value with the contact probability. Finally, the ABC scores were normalised for each enhancer by the sum of the ABC scores for all the enhancers and promoter. For each enhancer, the interaction with the highest ABC score was selected, filtering for expressed genes only (>1 TPM in at least one condition) (Tables S2 and S3). Gene Ontology Biological Process enrichment for the annotated genes was performed using the Bioconductor package clusterProfiler,[89] one-sided Fisher's exact test was applied with a p-adjust <0.05 as a cut-off, no assumptions about the underlying distribution of gene expression data was done. Pearson's correlation coefficient was determined between the enhancer profile and the gene expression profile. Statistical differences were calculated using one-way analysis of variance (ANOVA) with Tukey's HSD for multiple comparisons (p-value <0.05). To identify gene expression differences between the *de novo*, increasing and decreasing RRE-associated candidate target genes, two-way ANOVA with Tukey's HSD test for multiple comparisons was performed for each type of element (promoter, proximal and distal) (p-value <0.05).

Single-cell RNA sequencing analysis

The single-cell RNA-seq dataset generated from mouse livers collected at 0, 24 and 48 h post-PHx was retrieved from GEO: GSE151309.[31] The standard 10× Genomics Cell Ranger output was downloaded and imported using the Read10× function in Seurat v5.0.3.[98] The genes detected in 10 or fewer cells were filtered out. Cells with unique gene counts exceeding 500 for PHx0, 300 for PHx24, and 200 for PHx48 were retained, while cells with total gene counts above 4,000 or a mitochondrial gene percentage greater than 30% were filtered out. Seurat objects were then normalised and scaled to remove unwanted sources of variation, enhancing comparability among the samples. The top 2,000 variable genes were identified using the FindVariableFeatures function in Seurat for subsequent principal component analysis (PCA). To address potential batch effects, the RunHarmony function of Harmony v1.2.0[99] was applied to integrate the merged Seurat object. The clustering of cells was performed using the FindNeighbors and FindClusters functions in Seurat with a resolution parameter set to 0.4. Dimensionality reduction was achieved through Uniform Manifold Approximation and Projection (UMAP). Cell clusters were annotated based on the expression of marker genes in accordance with Chembazhi et al. (2021).[31] Visualisation plots were generated using scCustomize v2.1.2 to facilitate interpretation and analysis.

Transcription factor motif enrichment analysis

TF differential binding analysis was performed with HINT-ATAC,[47] a computational footprinting tool tailored for ATAC-seq data. As input, BAMs of biological replicate samples were merged with SAMtools v.1.16[100] and differentially accessible peaks were used as input regions for each time point. The resulting footprints were searched for motif enrichment using the HOCOMOCO v11 database. The analysis focused exclusively on the TFs expressed in the RNA-seq data (>1 TPM). Only the TF motifs with a HINT-ATAC absolute fold change activity value greater than 1.5 and an associated p-value <0.05 were considered significant (visualised by volcano plots). TF footprints were also visualised as lineplots, showing the mean of the ATAC-seq signal (adjusted for Tn5 cutting-bias) in the 200 bp window centered at each occupied motif.

For TF motif analysis, the Analysis of Motif Enrichment (AME) tool from the MEME suite v5.4.1[49] was used, using the HOCOMOCO v11 database and default parameters. To check for differential TF binding between the promoter and enhancer regulatory elements, the peaks located within 500 bp upstream or downstream of the transcriptional start site were considered promoter peaks and the rest were considered putative enhancer peaks. Only the TFs that were significantly enriched (Mann–Whitney U test, p-adjust <0.05) and expressed in the RNA-seq data (>1 TPM) were considered a hit, with the redundant hits removed. Only the top 10 TF motifs for each time point and peak class were represented in the heatmaps from Figure 4C.

Gene coexpression regulatory network

To construct the early regeneration gene coexpression regulatory network (GRN), we computed the correlation of expression across all samples between target genes linked to RREs (RRE-linked targets) and potential regulatory TFs, based on the presence of their motifs within these RREs. The GRN was generated using the expression values of 1,805 RRE-linked targets and 37 TFs. Only TF-target gene pairs containing the TF motif present in the RRE and those with absolute values of Pearson's correlation coefficient equal to or higher than 0.8 were considered as reliable. The resulting GRN included 1,829 nodes, of which 37 were source nodes (selected TFs), interconnected by 3,794 edges representing *de novo*, increasing and decreasing regulatory interactions. Network visualisation was performed using Cytoscape Software v3.10.2.[101] Nodes were displayed according to Edge-weighted Spring-Embedded Layout analysis of TF-target correlation of expression (Pearson's correlation coefficient between TF and target expression). Node size was adjusted to denote TFs and colored by normalised expression values calculated as z-scores for each time point. Edges were colored depending on TF-target correlation of expression (negative or positive) or based on RREs classification at each time point. Edge transparency was adjusted depending on RRE classification at each time point for visualisation purposes (Non-differentially accessible peaks were made more transparent).

Developmental analysis

To determine if the regeneration enhancers were repurposed from development, ATAC-seq data from mouse livers at different embryonic stages were obtained from the ENCODE development series ENCSR326DKM.[58] The ATAC-seq postnatal dataset was obtained from the reference epigenome ENCSR687SNT.[58] Peak coordinates were converted from mm10 to mm39 using the liftOver tool from the UCSC Genome Browser. *De novo* peaks overlapping open regions in the fetal or postnatal day 0 livers were considered to be reused. This overlap was calculated using BEDTools2 intersectBed.

QUANTIFICATION AND STATISTICAL ANALYSIS

The quantitative and statistical analyses are described in the relevant sections of the method details or in the figure legends.